Reliable Density-Functional-Theory Calculations of Adsorption in Nanoscale Pores

Robert W. Maier and Mark A. Stadtherr[1]

Department of Chemical Engineering
University of Notre Dame
Notre Dame, IN 46556
USA

January 2001
(revised, March 2001)

Topical Heading: Thermodynamics

Keywords: Adsorption, Density Functional Theory, Computational Method, Nanoporous Materials, Interval Analysis

[1]Author to whom all correspondence should be addressed; Fax: (219) 631-8366; Phone: (219) 631-9318; E-mail: markst@nd.edu

Abstract

A popular approach for the modeling of adsorption phenomena is density-functional theory (DFT). A new methodology is described that is the first *completely reliable* technique for finding *all* solutions to the nonlinear equation systems arising in the lattice-DFT modeling of adsorption in porous materials. The method is based on interval analysis, in particular an interval Newton/generalized bisection algorithm, which provides a mathematical and computational *guarantee* that all solutions are enclosed. The method is demonstrated using a model, formulated using DFT for a confined lattice, of adsorption in slit-like nanoscale pores. On several test problems, in addition to confirming solutions found previously, the method also found a number of additional, previously unreported solutions.

1 Introduction

The study of adsorption in porous materials has important applications in fields such as separation and purification, reaction and catalysis, the storage of gases, as well as many others. One popular approach for the modeling of adsorption phenomena is density-functional theory (DFT), which provides the capability to predict adsorption isotherms and phase behavior in the pore, including phase transitions (e.g., wetting, capillary condensation) and hysteresis effects.

The basic idea in formulating a DFT model is to represent the Helmholtz free energy F of the system as a functional of the density distribution $\rho(r)$; that is $F = F[\rho(r)]$, where r indicates some spatial coordinate(s). The density distribution $\rho(r)$ may be treated as continuous or as discrete. The latter is characteristic of a lattice model, as used in the example problems considered below. The equilibrium density distribution is then found by formulating and solving an appropriate minimization problem. For the case most often considered, that of constant temperature, pressure and chemical potentials (the grand canonical ensemble), the problem is to minimize the grand potential function $\Omega[\rho(r)]$. Alternatively (e.g., Neimark and Ravikovitch, 1998, 2000), one may consider the case of constant temperature, volume and mole numbers (the canonical ensemble). In this case, the problem is to minimize the Helmholtz free energy $F = F[\rho(r)]$ subject to the mole number constraints. In either case, the minimization problem is typically solved by converting the problem into an equivalent system of nonlinear equations, which is then solved for the equilibrium density distribution, from which an adsorption isotherm can be determined. For some situations, the relevant system of equations can be solved analytically in the form of an infinite series (e.g., Delmas and Patterson, 1960; Bellemans, 1962; Altenberger and Stecki, 1970). However, in other situations, especially in regions of phase transitions and hysteresis effects, which are often the regions of most interest, the equation system to be solved has multiple solutions (e.g., Aranovich and Donohue, 1999; Neimark and Ravikovitch, 1998, 2000; Lastoskie et al., 1993), and thus solving

the system is not straightforward. The multiple roots represent stationary points (local minima, local maxima, or saddle points) in the optimization problem. Local minima correspond to stable and metastable states in the adsorption problem being modeled, and local maxima and saddle points to unstable states. To fully understand the predictions of the DFT model, it is necessary to find *all* the stable and metastable states, and the unstable states may also be of some interest (e.g., Neimark and Ravikovitch, 1998). As emphasized by Aranovich and Donohue (1999), failure to find all the stationary points may not only result in the loss of important information, but also an incorrect or distorted view of the adsorption isotherm predicted by the model. Thus, there is a clear need for a nonlinear equation solving method capable of reliably finding *all* the stationary points.

One common approach to finding all the stationary points is to use multiple initial guesses in connection with some local equation solving technique, such as successive substitution, Newton, or quasi-Newton (Broyden) methods (e.g., Neimark and Ravikovitch, 1998). Using this type of approach, it is impossible to guarantee that all solutions will be found. A more reliable approach in many situations is the method of Aranovich and Donohue (1998, 1999). This is a "path tracking" (homotopy-continuation) approach that is very reliable for finding solutions lying along a single continuous path. However, it may not find solutions that lie on different paths, and so again it is impossible to guarantee that all solutions will be found.

We describe here a new approach to the problem of finding all solutions to the nonlinear equation system arising in DFT modeling of adsorption in porous materials. This technique is based on interval analysis, in particular, an interval-Newton generalized-bisection (IN/GB) algorithm. This method is *mathematically and computationally guaranteed* to enclose any and all solutions of a system of nonlinear equations. Here, this means that all density distributions that correspond to a stationary point in the optimization problem arising from DFT will be located.

To demonstrate this method, we use the lattice-DFT model of Aranovich and Donohue (1999)

for adsorption in nanoscale pores, which is based on the approach of Ono and Kondo (1960). Since Aranovich and Donohue use this model to demonstrate their path tracking algorithm, this means that a direct comparison can be made between their solution method and the new approach described here. In the next section, we summarize the model used and present the mathematical formulation of the problem. In Section 3, we describe the IN/GB algorithm used to solve for the stationary points. Then, in Section 4, we present results for several test problems, and, in Section 5, summarize our conclusions.

2 Problem Formulation: DFT for a Confined Lattice

The problem considered here is adsorption in a slit-like, nanoscale pore using DFT for a confined lattice. The model used is that described by Aranovich and Donohue (1999), who consider the one-dimensional density distribution in a lattice confined between two planes. As formulated by Aranovich and Donohue (1999), the model is for a binary mixture of molecules of A and B. However, since all the examples used here (and by Aranovich and Donohue) are for the special case of a single component system (B = holes), we will summarize here the problem formulation for this case.

Consider a pure component (A) distributed on a fixed lattice with N layers. Each site on each layer $i = 1, \ldots, N$ may either be occupied by a molecule of A or may be empty. The lattice is bound on both sides by adsorbate surfaces on the planes of $i = 0$ and $i = N + 1$. Since the adsorbant walls are identical, the system is symmetric. Thus, for a system with an even number of layers (the case for all example problems considered; if the number of layers is odd, the probably formulation is only slightly different), there are $n = N/2$ independent layer densities to be determined. An expression for the free energy $F = \mathcal{H} - TS$ of the system can be derived by determining the Hamiltonian $\mathcal{H}$ and the entropy S for the fluid confined in the lattice. Following Aranovich and Donohue, this is

done using a mean field approximation (Ono and Kondo, 1960) yielding

$$\mathcal{H} = 2\varepsilon_{\mathrm{AS}}\rho_1 + \sum_{i=1}^{n} z_2\varepsilon_{\mathrm{AA}}\rho_i^2 + \sum_{i=1}^{n-1} 2z_1\varepsilon_{\mathrm{AA}}\rho_i\rho_{i+1} + z_1\varepsilon_{\mathrm{AA}}\rho_n^2 \tag{1}$$

and

$$S = -k\sum_{i=1}^{n} 2\left[\rho_i \ln\rho_i + (1-\rho_i)\ln(1-\rho_i)\right]. \tag{2}$$

Here ρ_i is the density of A in layer i, expressed as the fraction of lattice sites in layer i which are occupied by a molecule of A, $\varepsilon_{\mathrm{AS}}$ and $\varepsilon_{\mathrm{AA}}$ are, respectively, the energies for adsorbate-surface and adsorbate-adsorbate interactions, and z_1 and z_2 are, respectively, the interlayer and intralayer coordination numbers (note that $2z_1+z_2$ will give the coordination number for the three-dimensional lattice). Using Eq. (1) for the Hamiltonian and Eq. (2) for the entropy, the reduced free energy $F_r = F/kT$ of the system can be expressed as

$$F_r = 2E_{\mathrm{AS}}\rho_1 + z_1E_{\mathrm{AA}}\rho_n^2 + \sum_{i=1}^{n} z_2E_{\mathrm{AA}}\rho_i^2 + \sum_{i=1}^{n-1} 2z_1E_{\mathrm{AA}}\rho_i\rho_{i+1} + \sum_{i=1}^{n} 2[\rho_i\ln\rho_i + (1-\rho_i)\ln(1-\rho_i)], \tag{3}$$

where E_{AA} and E_{AS} represent $\varepsilon_{\mathrm{AA}}/kT$ and $\varepsilon_{\mathrm{AS}}/kT$ respectively, and k is Boltzmann's constant.

We now seek to find the equilibrium density distribution under conditions of constant temperature, volume and mole numbers. To do this, values of $\rho_i, i = 1, \ldots, n$ must be found which minimize F_r under the constraint

$$N_{\mathrm{S}}\sum_{i=1}^{n} 2\rho_i = N_{\mathrm{A}}, \tag{4}$$

where N_{S} is the total number of lattice sites and N_{A} is the total number of A molecules in the system. To solve this problem, we seek stationary points of the Lagrangian function

$$\mathcal{L}(\boldsymbol{\rho}, \mu) = F_r(\boldsymbol{\rho}) - \mu\left[-\frac{N_A}{N_S} + \sum_{i=1}^{n} 2\rho_i\right], \tag{5}$$

where $\boldsymbol{\rho} = (\rho_1, \rho_2, \ldots, \rho_n)^{\mathrm{T}}$ is the density distribution vector and μ is a Lagrange multiplier that at the equilibrium state corresponds to the chemical potential. For $2 \le i \le n-1$, the stationarity condition is

$$\frac{\partial\mathcal{L}}{\partial\rho_i} = z_2E_{\mathrm{AA}}\rho_i + z_1E_{\mathrm{AA}}\rho_{i+1} + z_1E_{\mathrm{AA}}\rho_{i-1} + [\ln\rho_i - \ln(1-\rho_i)] - \mu = 0, \tag{6}$$

from which follows

$$\mu = z_2 E_{\mathrm{AA}} \rho_i + z_1 E_{\mathrm{AA}} \rho_{i+1} + z_1 E_{\mathrm{AA}} \rho_{i-1} + \ln(\frac{\rho_i}{1-\rho_i}). \tag{7}$$

Since μ corresponds to the chemical potential at the equilibrium state, and since the layers in the pore are assumed to be in equilibrium with the bulk, Eq. (7) must hold when $\rho_i = \rho_{i-1} = \rho_{i+1} = \rho_{\mathrm{b}}$, where ρ_{b} is the bulk density (mole fraction) of A. Thus, expressing μ in terms of ρ_{b} in Eq. (6) yields

$$\ln[\frac{\rho_i(1-\rho_{\mathrm{b}})}{\rho_{\mathrm{b}}(1-\rho_i)}] + z_2 E_{\mathrm{AA}}(\rho_i - \rho_{\mathrm{b}}) + z_1 E_{\mathrm{AA}}(\rho_{i+1} - \rho_{\mathrm{b}}) + z_1 E_{\mathrm{AA}}(\rho_{i-1} - \rho_{\mathrm{b}}) = 0. \tag{8}$$

Following a similar procedure for the case of $i = 1$, we can obtain

$$\ln[\frac{\rho_1(1-\rho_{\mathrm{b}})}{\rho_{\mathrm{b}}(1-\rho_1)}] + z_2 E_{\mathrm{AA}}(\rho_1 - \rho_{\mathrm{b}}) + z_1 E_{\mathrm{AA}}(\rho_2 - \rho_{\mathrm{b}}) - z_1 E_{\mathrm{AA}} \rho_{\mathrm{b}} + E_{\mathrm{AS}} = 0, \tag{9}$$

and, for the case of $i = n$,

$$\ln[\frac{\rho_n(1-\rho_{\mathrm{b}})}{\rho_{\mathrm{b}}(1-\rho_n)}] + z_2 E_{\mathrm{AA}}(\rho_n - \rho_{\mathrm{b}}) + z_1 E_{\mathrm{AA}}(\rho_n - \rho_{\mathrm{b}}) + z_1 E_{\mathrm{AA}}(\rho_{n-1} - \rho_{\mathrm{b}}) = 0. \tag{10}$$

Eqs. (8–10) constitute a nonlinear equation system of n equations in n unknowns. Given values of the coordination numbers z_1 and z_2, energy parameters E_{AS} and E_{AA}, and bulk density ρ_{b}, this equation system can be solved for the density distribution vector $\boldsymbol{\rho} = (\rho_1, \rho_2, \ldots, \rho_n)^{\mathrm{T}}$ describing the fractions of A in each of the N layers (remember that $\rho_1 = \rho_N, \rho_2 = \rho_{N-1}$, etc.). As discussed above, for problems of interest, due to presence of phase transitions or hysteresis effects, this equation system may have multiple solutions, all of which need to be found. We next describe a solution method that is *guaranteed* to enclose all the roots of this equation system.

3 Solution Method

We apply here interval mathematics, in particular an interval Newton/generalized bisection (IN/GB) technique, to find enclosures for all solutions to the problem defined above. We will very

briefly discuss these topics here, as well as explain how they were applied to solve the specific problem of interest. Recent monographs which more thoroughly introduce interval analysis, as well as interval arithmetic and other aspects of computing with intervals, include those of Neumaier (1990), Hansen (1992) and Kearfott (1996).

A real interval X is defined by $X = [x^{\mathrm{L}}, x^{\mathrm{U}}] = \{x \in \Re \mid x^{\mathrm{L}} \leq x \leq x^{\mathrm{U}}\}$. In other words, the interval X contains the section of the real number line bounded by the values x^{L} and x^{U}. A real interval vector $\mathbf{X} = (X_1, X_2, ..., X_n)^{\mathrm{T}}$ has n real interval components and since it can be interpreted geometrically as an n-dimensional rectangle, is frequently referred to as a *box*. Note that in this section lower case quantities are real numbers and upper case quantities are intervals. For an arbitrary function $\mathbf{f}(\mathbf{x})$, the *interval extension*, $\mathbf{F}(\mathbf{X}) \supseteq \{\mathbf{f}(\mathbf{x}) \mid \mathbf{x} \in \mathbf{X}\}$, encloses all values of $\mathbf{f}(\mathbf{x})$ for $\mathbf{x} \in \mathbf{X}$; that is, it encloses the *range* of $\mathbf{f}(\mathbf{x})$ over $\mathbf{X}$. It is often computed by substituting the given interval $\mathbf{X}$ into the function $\mathbf{f}(\mathbf{x})$ and then evaluating the function using interval arithmetic. The so-called "natural" interval extension so determined is often wider than the actual range of function values, but it always includes the actual range. The issue of computing interval extensions for the functions of interest here is considered in more detail below.

3.1 Interval Newton Method

Consider the solution of a nonlinear equation system $\mathbf{f}(\mathbf{x}) = \mathbf{0}$ where $\mathbf{x} \in \mathbf{X}^{(0)}$. The solution algorithm is applied to a sequence of intervals, beginning with the initial interval vector (box) $\mathbf{X}^{(0)}$ specified by the user. This initial interval can be chosen to be sufficiently large to enclose all physically feasible behavior. The basic iteration step in interval Newton methods is, given an interval $\mathbf{X}^{(k)}$ in the iteration sequence, to solve the linear interval equation system

$$F'(\mathbf{X}^{(k)})(\mathbf{N}^{(k)} - \mathbf{x}^{(k)}) = -\mathbf{f}(\mathbf{x}^{(k)}) \tag{11}$$

for a new interval $\mathbf{N}^{(k)}$, where k is an iteration counter, $F'(\mathbf{X}^{(k)})$ is an interval extension of the real Jacobian $f'(\mathbf{x})$ of $f(\mathbf{x})$ over the current interval $\mathbf{X}^{(k)}$, and $\mathbf{x}^{(k)}$ is a point in the interior of $\mathbf{X}^{(k)}$. It

can be shown (Moore, 1966) that any root $\mathbf{x}^* \in \mathbf{X}^{(k)}$ is also contained in the *image* $\mathbf{N}^{(k)}$, implying that if there is no intersection between $\mathbf{X}^{(k)}$ and $\mathbf{N}^{(k)}$, then no root exists in the box $\mathbf{X}^{(k)}$, and suggesting the iteration scheme $\mathbf{X}^{(k+1)} = \mathbf{X}^{(k)} \cap \mathbf{N}^{(k)}$. In addition to this iteration step, which can be used to tightly enclose a solution, the following property can be proven (e.g., Neumaier, 1990; Kearfott, 1996): If $\mathbf{N}^{(k)}$ is contained completely within $\mathbf{X}^{(k)}$, then there is *one and only one* root contained in $\mathbf{X}^{(k)}$, and it is in $\mathbf{N}^{(k)}$. This property is quite powerful, as it provides a *mathematical guarantee* of existence and uniqueness when it is satisfied.

The foregoing suggests a *root inclusion test* for $\mathbf{X}^{(k)}$:

1. (Range Test) Compute an interval extension $\mathbf{F}(\mathbf{X}^{(k)})$ containing the range of $\mathbf{f}(\mathbf{x})$ over $\mathbf{X}^{(k)}$ and test to see whether it contains zero. Clearly, if $0 \notin \mathbf{F}(\mathbf{X}^{(k)}) \supseteq \{\mathbf{f}(\mathbf{x}) \mid \mathbf{x} \in \mathbf{X}^{(k)}\}$ then there can be no solution of $\mathbf{f}(\mathbf{x}) = \mathbf{0}$ in $\mathbf{X}^{(k)}$ and this interval need not be further tested. Otherwise, if $\mathbf{0} \in \mathbf{F}(\mathbf{X}^{(k)})$, then the processing of $\mathbf{X}^{(k)}$ continues.

2. (Domain Reduction) In this step a simple *domain reduction* technique is used to try to reduce the size of $\mathbf{X}^{(k)}$. The method used in this step is sometimes referred to as *constraint propagation*, especially in the context of optimization problems. The basic idea is to rewrite one or more of the equations in the system in the form $x_i = g_i(\mathbf{x})$. For example, we can rewrite Eq. (9) as

$$\rho_2 = 2z_1 E_{AA}\rho_b - E_{AS} - z_2 E_{AA}(\rho_1 - \rho_b) - \ln[\frac{\rho_1(1-\rho_b)}{\rho_b(1-\rho_1)}]z_1 E_{AA} \tag{12}$$

and can do similar rearrangements with the other equations. Once the rearrangement to $x_i = g_i(\mathbf{x})$ has been done, we can then calculate a new range for x_i by substituting the current interval $\mathbf{X}^{(k)}$ into the expression for g_i, thus obtaining $X_{i,\text{calc}}^{(k)} = G_i(\mathbf{X}^{(k)})$. The range for x_i can now be reduced in many cases by using the intersection of the original range $X_i^{(k)}$ and the calculated range $X_{i,\text{calc}}^{(k)}$; that is $X_i^{(k)} \leftarrow X_i^{(k)} \cap X_{i,\text{calc}}^{(k)}$. If desired, this domain reduction step can be iterated until there is no further reduction in $\mathbf{X}^{(k)}$; however, for the

problems solved here, our tests indicate that, in terms of CPU time, a single pass is most effective.

3. (Interval Newton Test) Compute the image $\mathbf{N}^{(k)}$ by solving Eq. (11). There are now three possible outcomes:

   (a) If $\mathbf{X}^{(k)} \cap \mathbf{N}^{(k)} = \emptyset$, then there is no root in $\mathbf{X}^{(k)}$, and thus this interval need not be further tested.

   (b) If $\mathbf{N}^{(k)} \subset \mathbf{X}^{(k)}$, then there is exactly one root in $\mathbf{X}^{(k)}$ and since the number of roots in this interval is known, it need not be further tested. A rigorous enclosure of the root can be found by continuing the interval Newton iteration $\mathbf{X} \leftarrow \mathbf{X} \cap \mathbf{N}$, which will converge quadratically. Alternatively, an approximation of the root can be found using a standard point-valued Newton's method beginning from any point in $\mathbf{X}^{(k)}$.

   (c) If neither of the above is true, then no conclusion can be drawn about the number of roots in $\mathbf{X}^{(k)}$. However, if there are any roots in $\mathbf{X}^{(k)}$, they must be contained in the next interval Newton iterate $\mathbf{X}^{(k+1)} = \mathbf{X}^{(k)} \cap \mathbf{N}^{(k)}$. One can now repeat the root inclusion test on $\mathbf{X}^{(k+1)}$, assuming it is sufficiently smaller than $\mathbf{X}^{(k)}$, or one can bisect $\mathbf{X}^{(k+1)}$ and add the resulting two intervals to the sequence of intervals to be tested.

These are the basic ideas of interval Newton/generalized bisection (IN/GB) methods. As a framework for our implementation of the IN/GB method, we use appropriately modified FORTRAN-77 routines from the packages INTBIS (Kearfott and Novoa, 1990) and INTLIB (Kearfott *et al.*, 1994). In addition, for solving the interval Newton equation, the hybrid preconditioning technique of Gau et al. (1999) is employed. Overall, the IN/GB method described above provides a procedure that is mathematically *and* computationally guaranteed to enclose all solutions (density distributions) of the nonlinear equation system given by Eqs. (8–10).

3.2 Computing Interval Extensions

To achieve good efficiency in the solution method outlined above, it is desirable that the required interval extensions bound the corresponding function ranges as tightly as possible. As noted above, when interval arithmetic is used to obtain the natural interval extension, this often produces bounds that overestimate the actual range of the function. This is due to the "dependency" problem, which arises when a variable occurs more than once in a function expression. While a variable may have a range of *possible* values, it must take on a *unique* value each time it occurs in an expression. However, this type of dependency is not recognized when the natural interval extension is computed. In effect, when the natural interval extension is used, the range computed for the function is the range that would occur if each instance of a particular variable were allowed to take on a different value in its interval range.

For this particular problem, it is possible to eliminate the use of the natural interval extension and thus the dependency problem. This is possible because the bounds on the function ranges can be determined directly. This can be seen by looking at the derivatives of the functions in the system to be solved. From Eqs. (8–10), these are, for each function $i = 1, \ldots, n$,

$$\frac{\partial f_i}{\partial \rho_i} = \frac{1}{\rho_i} + \frac{1}{1-\rho_i} + k_1 \tag{13}$$

$$\frac{\partial f_i}{\partial \rho_{i-1}} = k_2 \quad (i \neq 1) \tag{14}$$

$$\frac{\partial f_i}{\partial \rho_{i+1}} = k_3 \quad (i \neq n), \tag{15}$$

where

$$k_1 = \begin{cases} z_2 E_{\mathrm{AA}} & : \quad i \neq n \\ (z_1 + z_2) E_{\mathrm{AA}} & : \quad i = n \end{cases}$$

and $k_2 = k_3 = z_1 E_{\mathrm{AA}}$ are constants whose value is determined by the physical parameters in the model.

Clearly, each function is monotonic with respect to ρ_{i-1} and ρ_{i+1}, and so the extrema of f_i will occur when these variables are at their bounds. With respect to ρ_i, the extrema of f_i will occur either when this variable is at its bounds or when it is at an interior point for which $\partial f_i/\partial \rho_i = 0$. Using Eq. (13), it can be shown that this latter condition is satisfied when

$$\rho_i = \frac{1 \pm \sqrt{1 + \frac{4}{k_1}}}{2}. \tag{16}$$

For $k_1 < -4$, this expression yields two real values for ρ_i. Thus, f_i has extrema at

$$\rho_i^- = \frac{1 - \sqrt{1 + \frac{4}{k_1}}}{2} \tag{17}$$

and

$$\rho_i^+ = \frac{1 + \sqrt{1 + \frac{4}{k_1}}}{2}. \tag{18}$$

Note that $0 < \rho_i^- < \frac{1}{2}$ and $\frac{1}{2} < \rho_i^+ < 1$ The nature of these extrema can be determined using

$$\frac{\partial^2 f_i}{\partial \rho_i^2} = -\frac{1}{\rho_i^2} + \frac{1}{(1-\rho_i)^2}. \tag{19}$$

Evaluation of the second derivative at ρ_i^- yields a negative result, so this point is a local maximum, and evaluation at ρ_i^+ yields a positive result, so this point is a local minimum. Furthermore, it can be seen that since the second derivative is zero at $\rho_i = \frac{1}{2}$ (and the third derivative is positive here), there is (for any k_1) a local minimum in the slope $\partial f_i/\partial \rho_i$ here and that minimum value of the slope is $4 + k_1$, which for the current range of k_1 being considered is negative. For $\rho_i \in [0, 1]$, which is the interval of interest, this is also a global minimum. However, since as either endpoint is approached, the slope is clearly positive, this means that the slope is negative only for $\rho_i^- < \rho_i < \rho_i^+$. For purposes of the discussion that follows, we will assume that ρ_i^- and ρ_i^+ are point values. However, as actually implemented, these are (very narrow) interval values computed using interval arithmetic, starting with degenerate (thin) intervals for the constants in Eqs. (17–18). This is necessary to maintain computational rigor.

Using this information about $\partial f_i/\partial \rho_i$ for $k_1 < -4$, and assuming that $E_{\rm AA} < 0$ so that f_i is monotonically decreasing with respect to both ρ_{i-1} and ρ_{i+1}, we can compute interval extensions of f_i over $[\boldsymbol{\rho}^{\rm L}, \boldsymbol{\rho}^{\rm U}] = ([\rho_1^{\rm L}, \rho_1^{\rm U}], [\rho_2^{\rm L}, \rho_2^{\rm U}], \ldots, [\rho_n^{\rm L}, \rho_n^{\rm U}])^{\rm T} \subseteq [\mathbf{0}, \mathbf{1}]$ as follows. For $\rho_i^{\rm U} \leq \rho_i^-$, f_i is monotonically increasing with respect to ρ_i, so

$$F_i([\boldsymbol{\rho}^{\rm L}, \boldsymbol{\rho}^{\rm U}]) = [f_i(\rho_{i-1}^{\rm U}, \rho_i^{\rm L}, \rho_{i+1}^{\rm U}), f_i(\rho_{i-1}^{\rm L}, \rho_i^{\rm U}, \rho_{i+1}^{\rm L})]. \tag{20}$$

For $\rho_i^{\rm L} \geq \rho_i^+$, f_i is also monotonically increasing with respect to ρ_i, so $F_i([\boldsymbol{\rho}^{\rm L}, \boldsymbol{\rho}^{\rm U}])$ can be computed from Eq. (20). For the case $\rho_i^- \leq \rho_i^{\rm L}$ and $\rho_i^{\rm U} \leq \rho_i^+$, f_i is monotonically decreasing with respect to ρ_i, so

$$F_i([\boldsymbol{\rho}^{\rm L}, \boldsymbol{\rho}^{\rm U}]) = [f_i(\rho_{i-1}^{\rm U}, \rho_i^{\rm U}, \rho_{i+1}^{\rm U}), f_i(\rho_{i-1}^{\rm L}, \rho_i^{\rm L}, \rho_{i+1}^{\rm L})]. \tag{21}$$

If $\rho_i^- \in [\rho_i^{\rm L}, \rho_i^{\rm U}]$ but $\rho_i^+ \notin [\rho_i^{\rm L}, \rho_i^{\rm U}]$, then there is an interior maximum of f_i with respect to ρ_i at ρ_i^- and either endpoint could be the minimum with respect to ρ_i; thus,

$$F_i([\boldsymbol{\rho}^{\rm L}, \boldsymbol{\rho}^{\rm U}]) = [\min\{f_i(\rho_{i-1}^{\rm U}, \rho_i^{\rm L}, \rho_{i+1}^{\rm U}), f_i(\rho_{i-1}^{\rm U}, \rho_i^{\rm U}, \rho_{i+1}^{\rm U})\}, f_i(\rho_{i-1}^{\rm L}, \rho_i^-, \rho_{i+1}^{\rm L})]. \tag{22}$$

If $\rho_i^+ \in [\rho_i^{\rm L}, \rho_i^{\rm U}]$ but $\rho_i^- \notin [\rho_i^{\rm L}, \rho_i^{\rm U}]$, then there is an interior minimum of f_i with respect to ρ_i at ρ_i^+ and either endpoint could be the maximum with respect to ρ_i; thus,

$$F_i([\boldsymbol{\rho}^{\rm L}, \boldsymbol{\rho}^{\rm U}]) = [f_i(\rho_{i-1}^{\rm U}, \rho_i^+, \rho_{i+1}^{\rm U}), \max\{f_i(\rho_{i-1}^{\rm L}, \rho_i^{\rm L}, \rho_{i+1}^{\rm L}), f_i(\rho_{i-1}^{\rm L}, \rho_i^{\rm U}, \rho_{i+1}^{\rm L})\}]. \tag{23}$$

Finally if $\rho_i^- \in [\rho_i^{\rm L}, \rho_i^{\rm U}]$ and $\rho_i^+ \in [\rho_i^{\rm L}, \rho_i^{\rm U}]$, then there are both an interior minimum and an interior maximum with respect to ρ_i, and

$$F_i([\boldsymbol{\rho}^{\rm L}, \boldsymbol{\rho}^{\rm U}]) = [\min\{f_i(\rho_{i-1}^{\rm U}, \rho_i^{\rm L}, \rho_{i+1}^{\rm U}), f_i(\rho_{i-1}^{\rm U}, \rho_i^+, \rho_{i+1}^{\rm U})\}, \max\{f_i(\rho_{i-1}^{\rm L}, \rho_i^{\rm U}, \rho_{i+1}^{\rm L}), f_i(\rho_{i-1}^{\rm L}, \rho_i^-, \rho_{i+1}^{\rm L})\}]. \tag{24}$$

As actually implemented, the bounding procedure is slightly more complex than described here, since it also accounts for the fact that ρ_i^- and ρ_i^+ must be treated as (very narrow) intervals.

For $k_1 = -4$, Eq. (16) yields one real value for ρ_i, namely $\rho_i = \frac{1}{2}$. Here the minimum slope is $4 + k_1 = 0$, which occurs at the inflection point $\rho_i = \frac{1}{2}$. For this case, f_i is monotonically

nondecreasing with respect to ρ_i, and for $[\boldsymbol{\rho}^{\mathrm{L}}, \boldsymbol{\rho}^{\mathrm{U}}] \subseteq [\mathbf{0}, \mathbf{1}]$, the computation of $F_i([\boldsymbol{\rho}^{\mathrm{L}}, \boldsymbol{\rho}^{\mathrm{U}}])$ can be done using Eq. (20).

For $-4 < k_1 < 0$, Eq. (16) yields no real roots, and for $k_1 > 0$ there are two real roots, but neither is in the interval $\rho_i \in [0, 1]$ of interest. Here the minimum slope is $4 + k_1 > 0$, so f_i is monotonically increasing and for $[\boldsymbol{\rho}^{\mathrm{L}}, \boldsymbol{\rho}^{\mathrm{U}}] \subseteq [\mathbf{0}, \mathbf{1}]$, the computation of $F_i([\boldsymbol{\rho}^{\mathrm{L}}, \boldsymbol{\rho}^{\mathrm{U}}])$ can be done using Eq. (20).

It is important to understand that when the endpoints of interval extensions are computed directly as in this fashion, each endpoint must be computed using interval arithmetic in order to maintain computational rigor. That is, if $f_i(\rho_{i-1}^{\mathrm{U}}, \rho_i^{\mathrm{L}}, \rho_{i+1}^{\mathrm{U}})$ is the lower endpoint of $F_i([\boldsymbol{\rho}^{\mathrm{L}}, \boldsymbol{\rho}^{\mathrm{U}}])$ then it is computed using interval arithmetic starting with the degenerate (thin) intervals $[\rho_{i-1}^{\mathrm{U}}, \rho_{i-1}^{\mathrm{U}}]$, $[\rho_i^{\mathrm{L}}, \rho_i^{\mathrm{L}}]$ and $[\rho_{i+1}^{\mathrm{U}}, \rho_{i+1}^{\mathrm{U}}]$, and the lower bound of the resulting interval is taken as the lower bound of $F_i([\boldsymbol{\rho}^{\mathrm{L}}, \boldsymbol{\rho}^{\mathrm{U}}])$. Similarly, if $f_i(\rho_{i-1}^{\mathrm{L}}, \rho_i^{\mathrm{U}}, \rho_{i+1}^{\mathrm{L}})$ is the upper endpoint of $F_i([\boldsymbol{\rho}^{\mathrm{L}}, \boldsymbol{\rho}^{\mathrm{U}}])$ then it is computed using interval arithmetic starting with the thin intervals $[\rho_{i-1}^{\mathrm{L}}, \rho_{i-1}^{\mathrm{L}}]$, $[\rho_i^{\mathrm{U}}, \rho_i^{\mathrm{U}}]$ and $[\rho_{i+1}^{\mathrm{L}}, \rho_{i+1}^{\mathrm{L}}]$, and the upper bound of the resulting interval is taken as the upper bound of $F_i([\boldsymbol{\rho}^{\mathrm{L}}, \boldsymbol{\rho}^{\mathrm{U}}])$. We also note that if $E_{\mathrm{AA}} > 0$, so that f_i is monotonically increasing with respect to ρ_{i-1} and ρ_{i+1}, instead of decreasing, as assumed before, the same procedure as outlined above can be used, except that all lower bounds will now be evaluated at ρ_{i-1}^{L} and ρ_{i+1}^{L} instead of ρ_{i-1}^{U} and ρ_{i+1}^{U}, and all upper bounds will be evaluated at ρ_{i-1}^{U} and ρ_{i+1}^{U} instead of ρ_{i-1}^{L} and ρ_{i+1}^{L}.

For use in Eq. (11), the interval Newton equation, it is also necessary to compute interval extensions of the Jacobian elements, which are given by Eqs. (13–15). The off-diagonal elements are all constants. For the diagonal elements $f'_{ii} = \partial f_i / \partial \rho_i$, it is clear from the discussion above that there is a minimum with respect to ρ_i at $\rho_i = \frac{1}{2}$. Furthermore, for $0 < \rho_i < \frac{1}{2}$, f'_{ii} is monotonically decreasing with respect to ρ_i, and for $\frac{1}{2} < \rho_i < 1$, f'_{ii} is monotonically increasing with respect to ρ_i. With this knowledge, the interval extensions F'_{ii} of the diagonal elements can be computed directly as follows. If $\rho_i^{\mathrm{U}} < \frac{1}{2}$, then $F'_{ii} = [f'_{ii}(\rho_i^{\mathrm{U}}), f'_{ii}(\rho_i^{\mathrm{L}})]$. If $\rho_i^{\mathrm{L}} > \frac{1}{2}$, then $F'_{ii} = [f'_{ii}(\rho_i^{\mathrm{L}}), f'_{ii}(\rho_i^{\mathrm{U}})]$. Finally,

if $\frac{1}{2} \in [\rho_i^{\mathrm{L}}, \rho_i^{\mathrm{U}}]$, then $F'_{ii} = [4 + k_1, \max\{f'_{ii}(\rho_i^{\mathrm{L}}), f'_{ii}(\rho_i^{\mathrm{U}})\}]$. Again, when the endpoints are computed directly, as done here, this must be done using interval arithmetic as explained above. Using the procedures described here, the necessary interval extensions of both functions and Jacobian elements can be computed *exactly* (within roundout), thus avoiding the overestimation that occurs when the natural interval extension is used. This can result in significant computational savings relative to using the natural interval extension. For example, for the example described below involving twenty layers ($N = 20$) and ten independent variables ($n = 10$), the savings in CPU time was about 80 percent.

4 Test Problems and Results

To demonstrate the use of the computational method proposed here, several test problems are considered. In each case, unless otherwise noted, the test problems were originally used by Aranovich and Donohue (1998,1999). This allows us to verify the ability of the proposed IN/GB technique to reliably enclose the previously found solutions. In several of the cases, however, IN/GB is able to find additional solutions which were not included in the previously published results. For each problem considered, the nonlinear equation system given by Eqs. (8–10) was solved using IN/GB for the density profile (layer concentrations) ρ_i, $i = 1, \ldots, n$, for many different values of the bulk concentration ρ_b. The results are then presented by plotting versus the bulk concentration. In solving the equation system, the initial intervals used for all the variables ρ_i was $[0, 1]$, thus the entire physically feasible variable space can be used as the initialization. Note that no initial point guess is needed, as in conventional equation solvers. All the computations were done on a Sun Ultra 10/440 workstation.

4.1 Two Layers

The first two problems have two layers ($N = 2$), so there is only one variable ($n = 1$) to

consider. These problems were originally presented in Aranovich and Donohue (1998). Figure 1 shows the results of solving the first problem, which is the case of $z_1 = 1$, $z_2 = 3$, $E_{\mathrm{AA}} = -1.4$ and $E_{\mathrm{AS}} = -1.0$. The plot gives the fraction ρ_1 $(= \rho_2)$ of lattice sites occupied by molecules of A as a function of the bulk mole fraction ρ_b of A. Note that this plot, and those given below, was prepared by solving the equation system for the layer concentration for a very large number of different values of the bulk concentration, and then plotting all the solutions; no curve fitting or smoothing techniques were used. For some values of the bulk concentration, the equation system has only one solution, but there are three ranges of ρ_b for which there are three roots. All the solutions lie on one continuous path. The solutions obtained agree closely with the plot presented by Aranovich and Donohue.

Figure 2 shows the results for another two-layer problem, this one with different energy parameters, $E_{\mathrm{AA}} = -1.9$ and $E_{\mathrm{AS}} = -0.258$, than the first. For this problem, using their path tracking approach, Aranovich and Donohue were able to find only the set of roots lying on the continuous path starting at the origin, which would suggest that, except for a small range at very high bulk concentration, there is only one root. Actually, however, for a large range of ρ_b, running from just above zero to about 0.5, there are three roots, which are very easily found using the IN/GB approach, but not found with the path tracking method. The difficulty for the path tracking approach is that the roots do not all lie on one continuous path. Aranovich and Donohue were well aware of this issue, and presented this example to show a case in which their approach would fail. This is one instance where IN/GB has the ability to find *all* of the solutions, wherever they may be located, while other techniques may not.

4.2 Four Layers

This test problem, and the remaining problems, are multivariable problems, many of which were originally examined by Aranovich and Donohue (1999). Rather than show the individual

layer results, we follow Aranovich and Donohue and give the Gibbs adsorption

$$\Gamma = \sum_{i=1}^{N} [\rho_i - \rho_b] = \sum_{i=1}^{n} 2[\rho_i - \rho_b]$$

as a function of the bulk concentration ρ_b. These adsorption isotherms also provide a convenient way to see the location and type of the phase transitions in the confined fluid.

For this four-layer problem, $z_1 = 1$, $z_2 = 4$, $E_{\mathrm{AA}} = -1.1$ and $E_{\mathrm{AS}} = -3.0$. Figure 3 shows the results of solving for the layer concentrations for a large number of bulk concentration values and then plotting the Gibbs adsorption isotherm; this result is in close agreement with that obtained by Aranovich and Donohue (1999). As seen in this plot, there are two ranges of bulk concentration for which the equation system has three roots. These multivalued regions correspond to phase transitions. As the bulk concentration of A is increased from zero, there is first a wetting transition in which the two layers nearest the pore walls fill. Then, at higher bulk concentration, there is a capillary condensation in which the remaining layers fill. The exact locations of the equilibrium phase transitions can be determined based on equality of spreading pressure, as shown by Aranovich and Donohue, and are not shown in the plot here. The plot does distinguish between solutions at which the Helmholtz energy surface is convex (bold curve), indicating a stable or metastable state, or nonconvex (non-bold curve), indicating an unstable state. This allows hysteresis effects to be easily seen. For example, in the capillary condensation transition, as the bulk concentration is increased through the transition, one may stay on the middle bold curve past the equilibrium transition until the metastable state disappears around $\rho_b = 0.035$, at which point there is a jump up to the topmost bold curve. But, as the bulk concentration is decreased through the transition, one may stay on the topmost bold curve past the equilibrium transition until this metastable state disappears around 0.019, and there is a jump down to the middle bold curve.

4.3 Eight Layers

In this set of problems, there are eight layers, so the number of independent variables is $n = 4$.

The first test problem considered, with $z_1 = 1$, $z_2 = 4$, $E_{\mathrm{AA}} = -1.4$ and $E_{\mathrm{AS}} = -4.0$, was also used by Aranovich and Donohue (1999). Figure 4 shows the results of solving for the ρ_i for a large number of ρ_b values and then plotting the Gibbs adsorption isotherm. This is another case where the benefits of the IN/GB approach can be clearly seen. The continuous track of roots which begins at the origin matches well with the track presented by the previous authors (though the roots shown by Aranovich and Donohue appear to be slightly off in places, especially near the origin). In addition to these solutions, however, the IN/GB approach finds another set of solutions (resembling a figure eight on the plot), which were not found previously. This demonstrates the ability of IN/GB to find *all* solutions to the problem. The results indicate that there is a wetting transition, as in the previous problem, in which layers one and eight (nearest the pore surface) are filled. As the bulk concentration is increased, this is followed by a capillary condensation transition in which all the remaining layers fill. This equilibrium transition "hides" two metastable states (bold curves) found on the continuous track of roots. The first, at about $\Gamma = 4$, corresponds to the filling of layer two (and seven), and the second, at about $\Gamma = 6$, corresponds to the filling of layer three (and six). In addition, there is also a metastable portion of the newly-found figure eight of roots. This appears to to be an "overhang" state, corresponding to the filling of layer three faster than layer two (and six faster than seven).

In addition to solving this first problem with the energy parameters used by Aranovich and Donohue, we have also solved the eight-layer case with some other energy parameter values. This demonstrates the ease with which the IN/GB approach can be used in modeling studies, here to determine the effect on the solution of changing the energy parameters. As a first such case, we change E_{AS} from -4.0 to -3.0, thus lowering the strength of the adsorption of A on the surface. The results, shown in Figure 5, shows that this has little effect on the overall character of the solution. However, not unexpectedly, the initial wetting transition now does not occur until higher values of the bulk concentration, reflecting the weaker strength of adsorption. For the remaining problems,

we set $E_{\mathrm{AS}} = -4.0$, and use different values of E_{AA}. First, E_{AA} is changed from the original -1.4 to -1.2, thus weakening the strength of the bonds between neighboring A molecules, with the result shown in Figure 6. One effect of doing this is that the equilibrium phase transitions now occur at larger values of the bulk concentration. However, it can also be seen that for this value of E_{AA}, the metastable overhang state disappears. Apparently, the bonds between neighboring molecules are now not strong enough to support any overhang of one layer over another. Increasing the bond strength slightly to $E_{\mathrm{AA}} = -1.3$, as shown in Figure 7, causes a small region of metastable overhang states to reappear. Finally, we significantly increase the bond strength to $E_{\mathrm{AA}} = -1.8$, with the result shown in Figure 8. Now the equilibrium phase transitions occur at smaller values of the bulk concentration. The bond strength is now sufficient to allow an additional metastable overhang state to occur, this one corresponding to layer four filling faster than layer three (and five faster than six).

4.4 Twelve Layers

For this case, there are 12 layers, so the number of independent variables is $n = 6$. For the problem considered, $z_1 = 1$, $z_2 = 4$, $E_{\mathrm{AA}} = -1.1$ and $E_{\mathrm{AS}} = -3.0$, as also used by Aranovich and Donohue (1999). Figure 9 shows the results. Again, the continuous track which begins at the origin matches closely the solution presented by Aranovich and Donohue. However, IN/GB has also located additional solutions not found by Aranovich and Donohue, just as in the previous set of problems.

4.5 Twenty Layers

The final problem we present involves 20 layers and 10 independent variables. The parameters used here and by Aranovich and Donohue (1999) are $z_1 = 1$, $z_2 = 4$, $E_{\mathrm{AA}} = -1.0$ and $E_{\mathrm{AS}} = -3.0$, and the results are shown in Figure 10, with an expanded view of part of the solution shown in

Figure 11. Again there is a continuous path of solutions beginning at the origin that closely matches what is given by Aranovich and Donohue. However, IN/GB also finds a large number of additional solutions to the equation system. Many of these are unstable states, but also found are a number of new metastable states, which can be interpreted in terms of overhang as discussed above. It may not be possible to observe all metastable states experimentally; however, as discussed in detail by Aranovich and Donohue (1999), knowledge of these states and the corresponding transitions is important in understanding the physical mechanisms underlying the phase behavior in the pore. In the region with most solutions, there are a total of 65 roots, only 15 of which lie in the continuous track that begins at the origin. The set of 65 solutions for the case $\rho_b = 0.068$ are listed in Table 1, for potential use by those who may wish to use this problem to test another equation solving technique. It should be noted that, while point approximations of the solutions, rounded to five decimal places, are reported here, we have actually determined rigorous interval enclosures of each solution. Each such enclosure is known to contain a *unique* root, based on the interval-Newton uniqueness test described above.

4.6 Computational Performance

Table 2 shows, as a function of problem size, the average CPU time required to obtain all solutions of the nonlinear equation system for a particular given value of the bulk concentration. Times are on a Sun Ultra 10/440 workstation. The results indicate that the IN/GB approach is remarkably efficient considering that it also provides a mathematical and computational guarantee that all the solutions have been found.

The larger average solution time for the larger problems is due mostly to the fact that, for the parameter values chosen, these have a larger number of solutions to be found. For the largest problem (20 layers), Figure 12 shows the relationship between the number of solutions and the computation time, by plotting both as a function of the bulk concentration value used. This shows

that IN/GB is very efficient when the number of solutions is small, taking more time only when many solutions exist and more work is required to enclose each solution uniquely.

5 Concluding Remarks

We have described here a new methodology that is the first *completely reliable* technique for finding *all* solutions to the nonlinear equation systems arising in the lattice-DFT modeling of adsorption in porous materials. The method is based on interval analysis, in particular an interval Newton/generalized bisection algorithm, which provides a mathematical and computational *guarantee* that all solutions are enclosed. The method was demonstrated using a number of test problems, finding not only the previously reported solutions, but also that these problems have additional unreported solutions. The new methodology is not only completely reliable, but it solved these problems very efficiently in terms of CPU requirements.

Acknowledgments — This work has been supported in part by the donors of The Petroleum Research Fund, administered by the ACS, under Grant 35979-AC9, by the National Science Foundation Grant EEC97-00537-CRCD, and by the Environmental Protection Agency Grant R826-734-01-0. We also thank Prof. Edward J. Maginn for his helpful comments and advice.

Literature Cited

Altenberger, A. R. and J. Stecki, "Surface Tension and Adsorption of Regular Solutions on the Solid-Liquid and Vapour-Liquid Interface," *Chem. Phys. Lett.*, **5**, 29 (1970).

Aranovich, G. L. and M. D. Donohue, "A Simple Numerical Algorithm for Solution of Non-linear Equations with Multiple Roots," *Comput. Chem.*, **22**, 429 (1998).

Aranovich, G. L. and M. D. Donohue, "Phase Loops in Density-Functional-Theory Calculations of Adsorption in Nanoscale Pores," *Phys. Rev. E*, **60**, 5552 (1999).

Bellemans, A., "Statistical Mechanics of Surface Phenomena–II. A Cluster Expansion of the Local Properties of the Surface Layer," *Physica*, **28**, 617 (1962).

Delmas, G. and D. Patterson, "Adsorption from Binary Solutions of Non-Electrolytes," *J. Phys. Chem.*, **64**, 1827 (1960).

Gau, C.-Y. R. W. Maier and M. A. Stadtherr, "New Interval Methodologies for Reliable Process Modeling," presented at AIChE Annual Meeting, paper 219g, Dallas, TX, November 1999.

Hansen, E. R., *Global Optimization Using Interval Analysis*, Marcel Dekkar, New York, NY (1992).

Kearfott, R. B., *Rigorous Global Search: Continuous Problems*, Kluwer, Dordrecht, The Netherlands (1996).

Kearfott, R. B. and M. Novoa III, "Algorithm 681: INTBIS, A Portable Interval-Newton / Bisection Package," *ACM Trans. Math. Softw.*, **16**, 152 (1990).

Kearfott, R. B., M. Dawande, K.-S. Du and C.-Y. Hu, "Algorithm 737: INTLIB, A Portable FORTRAN 77 Interval Standard Function Library," *ACM Trans. Math. Softw.*, **20**, 447 (1994).

Lastoskie, C., K. E. Gubbins and N. Quirke, "Pore Size Distribution Analysis of Microporous Carbons: A Density Functional Theory Approach." *J. Phys Chem.*, **97**, 4786 (1993).

Moore, R. E., *Interval Analysis*, Prentice-Hall, Englewood Cliffs, NJ (1966).

Neimark, A. V. and P. I. Ravikovitch, "Density Functional Theory for Studies of Multiple States of Inhomogeneous Fluids at Solid Surfaces and in Pores," in *Microscopic Simulation of Interfacial Phenomena in Solids and Liquids*, S. R. Phillpot, P. D. Bristowe, D. G. Stroud, J. R. Smith, Eds., *Materials Research Society Symposium Procedings*, Volume 492, Materials Research Society, Warrendale, Pennsylvania (1998).

Neimark, A. V. and P. I. Ravikovitch, "Density Functional Theory of Adsorption Hysteresis and Nanopore Characterization," in *Characterization of Porous Solids V*, K. K. Unger, G. Kreysa, J. P. Baselt, Eds., *Studies in Surface Science and Catalysis*, Volume 128, Elsevier, Amsterdam (2000).

Neumaier, A., *Interval Methods for Systems of Equations*, Cambridge Univ. Press, Cambridge, UK (1990).

Ono, S. and S. Kondo, "Molecular Theory of Surface Tension in Liquids," in *Encyclopedia of Physics*, S. Flügge, Ed., Volume 10, Springer-Verlag, Berlin (1960).

Table 1: List of the 65 solutions to the 20-layer problem at $\rho_b = 0.068$.

layer	sol 1	sol 2	sol 3	sol 4	sol 5	sol 6	sol 7	sol 8	sol 9	sol 10
1	0.99243	0.99243	0.99243	0.99243	0.99243	0.99243	0.99243	0.99243	0.99243	0.99240
2	0.93232	0.93232	0.93232	0.93232	0.93227	0.93231	0.93231	0.93230	0.93228	0.92775
3	0.92695	0.92695	0.92695	0.92694	0.92646	0.92693	0.92691	0.92672	0.92657	0.87502
4	0.92644	0.92644	0.92642	0.92641	0.92121	0.92622	0.92606	0.92404	0.92240	0.54408
5	0.92640	0.92635	0.92617	0.92601	0.87345	0.92400	0.92235	0.90151	0.88504	0.15127
6	0.92639	0.92590	0.92400	0.92233	0.54264	0.90150	0.88503	0.70987	0.60431	0.15198
7	0.92639	0.92124	0.90167	0.88491	0.15279	0.70986	0.60434	0.17959	0.14700	0.54750
8	0.92639	0.87432	0.71104	0.60362	0.15913	0.17958	0.14701	0.07846	0.07520	0.87442
9	0.92639	0.54700	0.18043	0.14701	0.57181	0.07846	0.07521	0.06890	0.06862	0.92125
10	0.92639	0.15206	0.07965	0.07591	0.86869	0.06898	0.06867	0.06808	0.06806	0.92586
layer	sol 11	sol 12	sol 13	sol 14	sol 15	sol 16	sol 17	sol 18	sol 19	sol 20
1	0.99243	0.99243	0.99243	0.99242	0.99242	0.99240	0.99242	0.99240	0.99243	0.99243
2	0.93188	0.93155	0.93175	0.93106	0.93039	0.92851	0.93033	0.92857	0.93224	0.93226
3	0.92186	0.91797	0.92031	0.91220	0.90451	0.88340	0.90383	0.88408	0.92609	0.92632
4	0.87438	0.83743	0.85937	0.78676	0.72577	0.58876	0.72072	0.59259	0.91735	0.91977
5	0.54668	0.39738	0.47809	0.27210	0.19150	0.14622	0.18715	0.14607	0.83720	0.85964
6	0.15199	0.18248	0.16640	0.16666	0.09377	0.08764	0.08787	0.08318	0.39720	0.47979
7	0.15212	0.39889	0.27079	0.47762	0.19078	0.18621	0.14727	0.14714	0.18268	0.16614
8	0.54729	0.83769	0.78565	0.85910	0.72398	0.71853	0.59269	0.59688	0.39962	0.26825
9	0.87427	0.91733	0.91133	0.91965	0.90342	0.90267	0.88289	0.88365	0.83761	0.78317
10	0.92071	0.92544	0.92481	0.92569	0.92396	0.92388	0.92169	0.92177	0.91632	0.90912
layer	sol 21	sol 22	sol 23	sol 24	sol 25	sol 26	sol 27	sol 28	sol 29	sol 30
1	0.99243	0.99243	0.99243	0.99243	0.99243	0.99242	0.99242	0.99240	0.99240	0.99243
2	0.93220	0.93213	0.93213	0.93196	0.93196	0.93024	0.93024	0.92867	0.92868	0.93211
3	0.92553	0.92476	0.92471	0.92274	0.92279	0.90283	0.90280	0.88522	0.88525	0.92458
4	0.91146	0.90348	0.90296	0.88306	0.88355	0.71331	0.71310	0.59910	0.59928	0.90161
5	0.78603	0.72367	0.71983	0.59257	0.59531	0.18127	0.18112	0.14592	0.14592	0.71008
6	0.27141	0.19040	0.18716	0.14709	0.14700	0.07968	0.07946	0.07608	0.07589	0.17966
7	0.16667	0.09314	0.08879	0.08727	0.08418	0.07912	0.07715	0.07872	0.07681	0.07846
8	0.47833	0.18701	0.15501	0.18221	0.15524	0.17533	0.15609	0.17497	0.15616	0.06890
9	0.85910	0.71508	0.62117	0.70827	0.62662	0.69706	0.63671	0.69641	0.63730	0.06808
10	0.91893	0.89868	0.88065	0.89753	0.88184	0.89559	0.88400	0.89548	0.88413	0.06801
layer	sol 31	sol 32	sol 33	sol 34	sol 35	sol 36	sol 37	sol 38	sol 39	sol 40
1	0.99243	0.99242	0.99240	0.99203	0.99194	0.99139	0.99137	0.99195	0.99202	0.99139
2	0.93198	0.93023	0.92869	0.88181	0.87061	0.80653	0.80389	0.87154	0.88105	0.80602
3	0.92294	0.90268	0.88539	0.51625	0.45779	0.23594	0.22968	0.46237	0.51199	0.23472
4	0.88507	0.71224	0.60005	0.14404	0.15482	0.10046	0.09310	0.15400	0.14479	0.09908
5	0.60393	0.18047	0.14591	0.15126	0.25146	0.19594	0.14740	0.24388	0.15860	0.18728
6	0.14691	0.07855	0.07510	0.55202	0.77432	0.72973	0.58799	0.76478	0.57795	0.70984
7	0.07519	0.06891	0.06861	0.87532	0.90996	0.90422	0.88213	0.90189	0.86979	0.89379
8	0.06862	0.06808	0.06805	0.92135	0.92481	0.92425	0.92204	0.87192	0.86783	0.87090
9	0.06805	0.06801	0.06800	0.92591	0.92624	0.92619	0.92598	0.55429	0.56660	0.55737
10	0.06800	0.06800	0.06800	0.92634	0.92637	0.92637	0.92635	0.15476	0.15959	0.15594

Table 1 continued

layer	sol 41	sol 42	sol 43	sol 44	sol 45	sol 46	sol 47	sol 48	sol 49	sol 50
1	0.99137	0.99237	0.99234	0.99239	0.99229	0.99209	0.99228	0.99209	0.99134	0.99134
2	0.80439	0.92412	0.91997	0.92639	0.91388	0.88861	0.91340	0.88908	0.80088	0.80074
3	0.23086	0.83667	0.79552	0.86044	0.73993	0.55590	0.73585	0.55882	0.22276	0.22245
4	0.09453	0.38868	0.28231	0.47663	0.19784	0.13816	0.19353	0.13784	0.08426	0.08383
5	0.15733	0.18157	0.16803	0.16531	0.09468	0.08661	0.08862	0.08227	0.08017	0.07669
6	0.62375	0.40512	0.47174	0.26872	0.19149	0.18549	0.14723	0.14706	0.18081	0.14701
7	0.87899	0.83960	0.85768	0.78451	0.72483	0.71766	0.59177	0.59744	0.71155	0.60284
8	0.86901	0.91755	0.91950	0.91121	0.90356	0.90258	0.88281	0.88382	0.90174	0.88477
9	0.56305	0.92555	0.92573	0.92493	0.92419	0.92409	0.92211	0.92221	0.92401	0.92231
10	0.15816	0.92630	0.92632	0.92624	0.92616	0.92615	0.92595	0.92596	0.92614	0.92597

layer	sol 51	sol 52	sol 53	sol 54	sol 55	sol 56	sol 57	sol 58	sol 59	sol 60
1	0.99228	0.99228	0.99210	0.99210	0.99134	0.99134	0.99228	0.99210	0.99228	0.99210
2	0.91275	0.91272	0.88987	0.88990	0.80048	0.80047	0.91266	0.88997	0.91266	0.88998
3	0.73026	0.73000	0.56365	0.56387	0.22187	0.22184	0.72950	0.56431	0.72949	0.56432
4	0.18798	0.18772	0.13735	0.13732	0.08306	0.08302	0.18725	0.13728	0.18723	0.13728
5	0.08044	0.08006	0.07529	0.07496	0.07022	0.06993	0.07934	0.07435	0.07932	0.07433
6	0.07973	0.07632	0.07916	0.07582	0.07860	0.07534	0.06984	0.06940	0.06968	0.06924
7	0.18046	0.14708	0.18005	0.14708	0.17965	0.14709	0.07802	0.07797	0.07621	0.07617
8	0.71103	0.60349	0.71046	0.60400	0.70990	0.60450	0.17434	0.17430	0.15629	0.15630
9	0.90163	0.88481	0.90155	0.88490	0.90147	0.88499	0.69527	0.69519	0.63835	0.63843
10	0.92376	0.92190	0.92376	0.92191	0.92375	0.92192	0.89528	0.89527	0.88435	0.88436

layer	sol 61	sol 62	sol 63	sol 64	sol 65
1	0.99134	0.99134	0.99228	0.99210	0.99134
2	0.80045	0.80045	0.91266	0.88998	0.80044
3	0.22179	0.22179	0.72943	0.56437	0.22179
4	0.08296	0.08295	0.18718	0.13728	0.08295
5	0.06937	0.06936	0.07924	0.07426	0.06929
6	0.06897	0.06881	0.06897	0.06854	0.06811
7	0.07792	0.07612	0.06808	0.06805	0.06801
8	0.17425	0.15631	0.06801	0.06800	0.06800
9	0.69511	0.63850	0.06800	0.06800	0.06800
10	0.89525	0.88438	0.06800	0.06800	0.06800

Table 2: Computational performance on test problems. The average solution time is the average CPU time required to obtain all solutions of the nonlinear equation system for a particular given value of the bulk concentration. Times are on a Sun Ultra 10/440 workstation.

Layers (N)	Variables ($N/2$)	Average Solution Time (s)
2	1	0.001
4	2	0.002
8	4	0.006
12	6	0.019
20	10	0.316

Figure Captions

Figure 1: Results for two-layer problem with $z_1 = 1, z_2 = 3, E_{AA} = -1.4, E_{AS} = -1.0$.

Figure 2: Results for two-layer problem with $z_1 = 1, z_2 = 3, E_{AA} = -1.9, E_{AS} = -0.258$.

Figure 3: Results for four-layer problem with $z_1 = 1, z_2 = 4, E_{AA} = -1.1, E_{AS} = -3.0$. The bold lines indicate regions that are either stable or metastable. The thin lines indicate unstable regions.

Figure 4: Results for eight-layer problem with $z_1 = 1, z_2 = 4, E_{AA} = -1.4, E_{AS} = -4.0$. The bold lines indicate regions that are either stable or metastable. The thin lines indicate unstable regions.

Figure 5: Results for eight-layer problem with $z_1 = 1, z_2 = 4, E_{AA} = -1.4, E_{AS} = -3.0$. The bold lines indicate regions that are either stable or metastable. The thin lines indicate unstable regions.

Figure 6: Results for eight-layer problem with $z_1 = 1, z_2 = 4, E_{AA} = -1.2, E_{AS} = -4.0$. The bold lines indicate regions that are either stable or metastable. The thin lines indicate unstable regions.

Figure 7: Results for eight-layer problem with $z_1 = 1, z_2 = 4, E_{AA} = -1.3, E_{AS} = -4.0$. The bold lines indicate regions that are either stable or metastable. The thin lines indicate unstable regions.

Figure 8: Results for eight-layer problem with $z_1 = 1, z_2 = 4, E_{AA} = -1.8, E_{AS} = -4.0$. The bold lines indicate regions that are either stable or metastable. The thin lines indicate unstable regions.

Figure 9: Results for 12-layer problem with $z_1 = 1, z_2 = 4, E_{AA} = -1.1, E_{AS} = -3.0$. The bold lines indicate regions that are either stable or metastable. The thin lines indicate unstable regions.

Figure 10: Results for 20-layer problem with $z_1 = 1, z_2 = 4, E_{AA} = -1.0, E_{AS} = -3.0$. The bold lines indicate regions that are either stable or metastable. The thin lines indicate unstable regions.

Figure 11: An expanded version of part of Figure 11 showing results for 20-layer problem. The bold lines indicate regions that are either stable or metastable. The thin lines indicate unstable regions.

Figure 12: Number of roots and computational performance on the 20-layer problem. Circles correspond to the left axis, and indicates the number of solutions at a particular bulk concentration. The line corresponds to the right axis, and indicates the time required to completely solve the problem for all the roots.

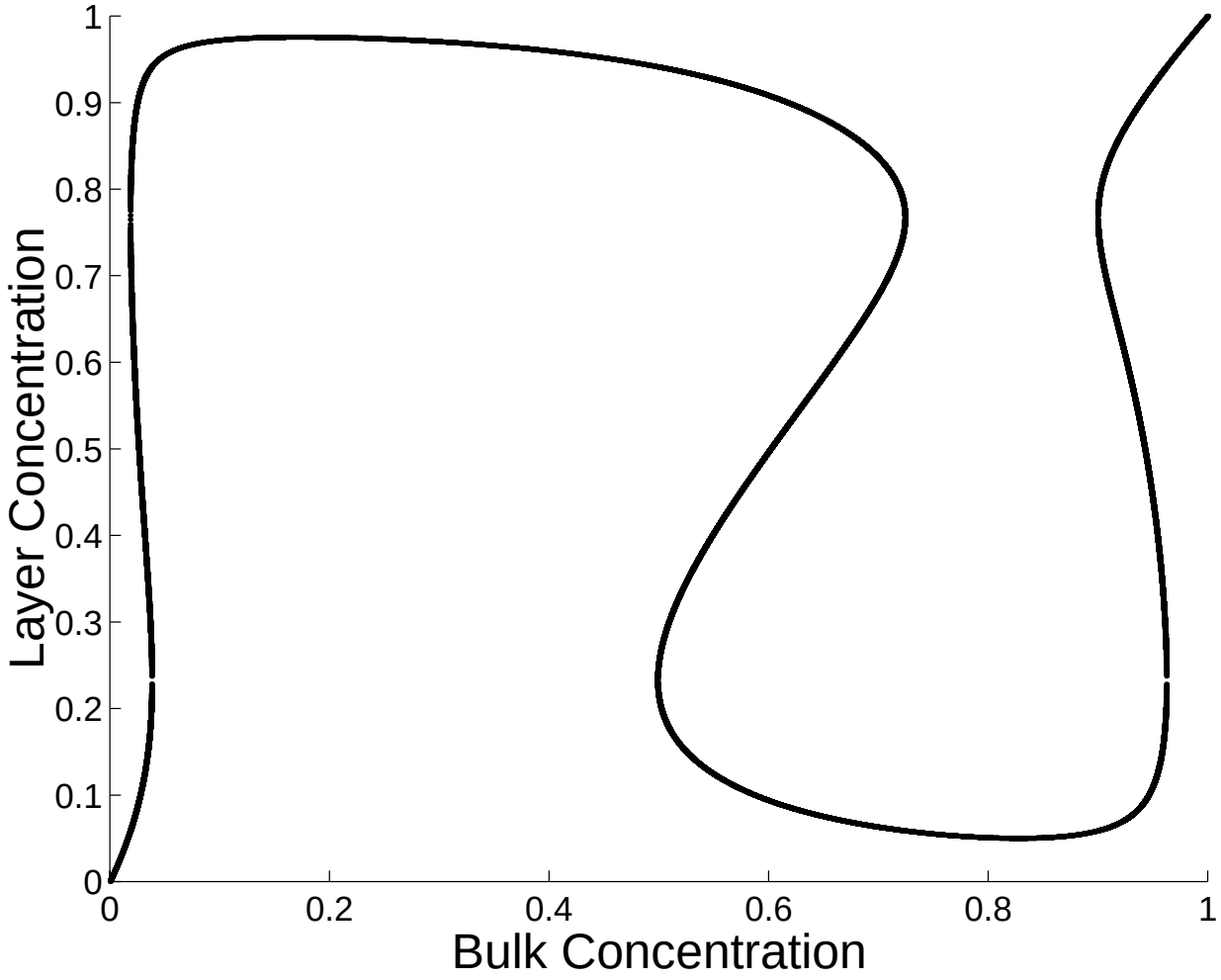

Figure 1: Results for two-layer problem with $z_1 = 1, z_2 = 3, E_{AA} = -1.4, E_{AS} = -1.0$.

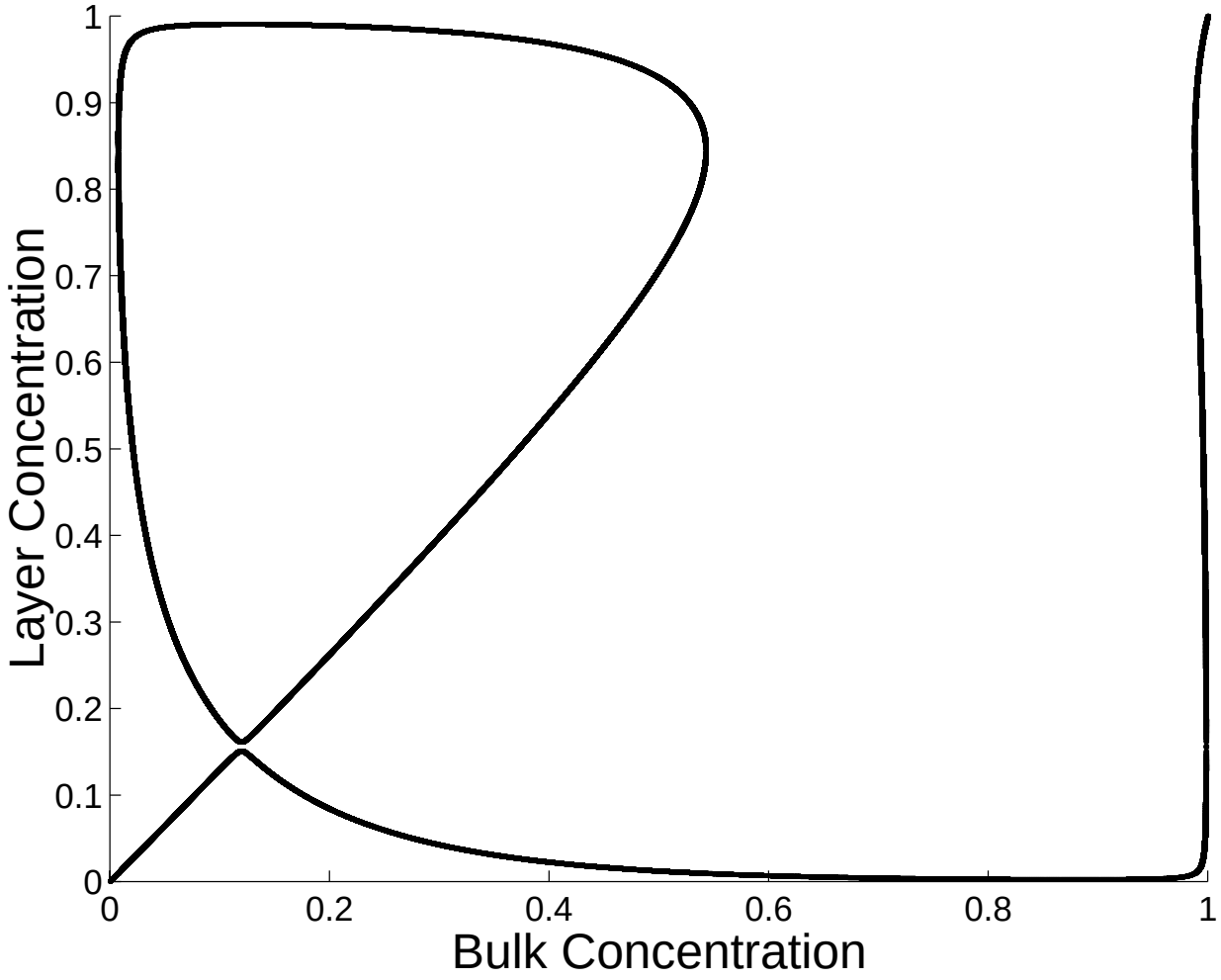

Figure 2: Results for two-layer problem with $z_1 = 1, z_2 = 3, E_{AA} = -1.9, E_{AS} = -0.258$.

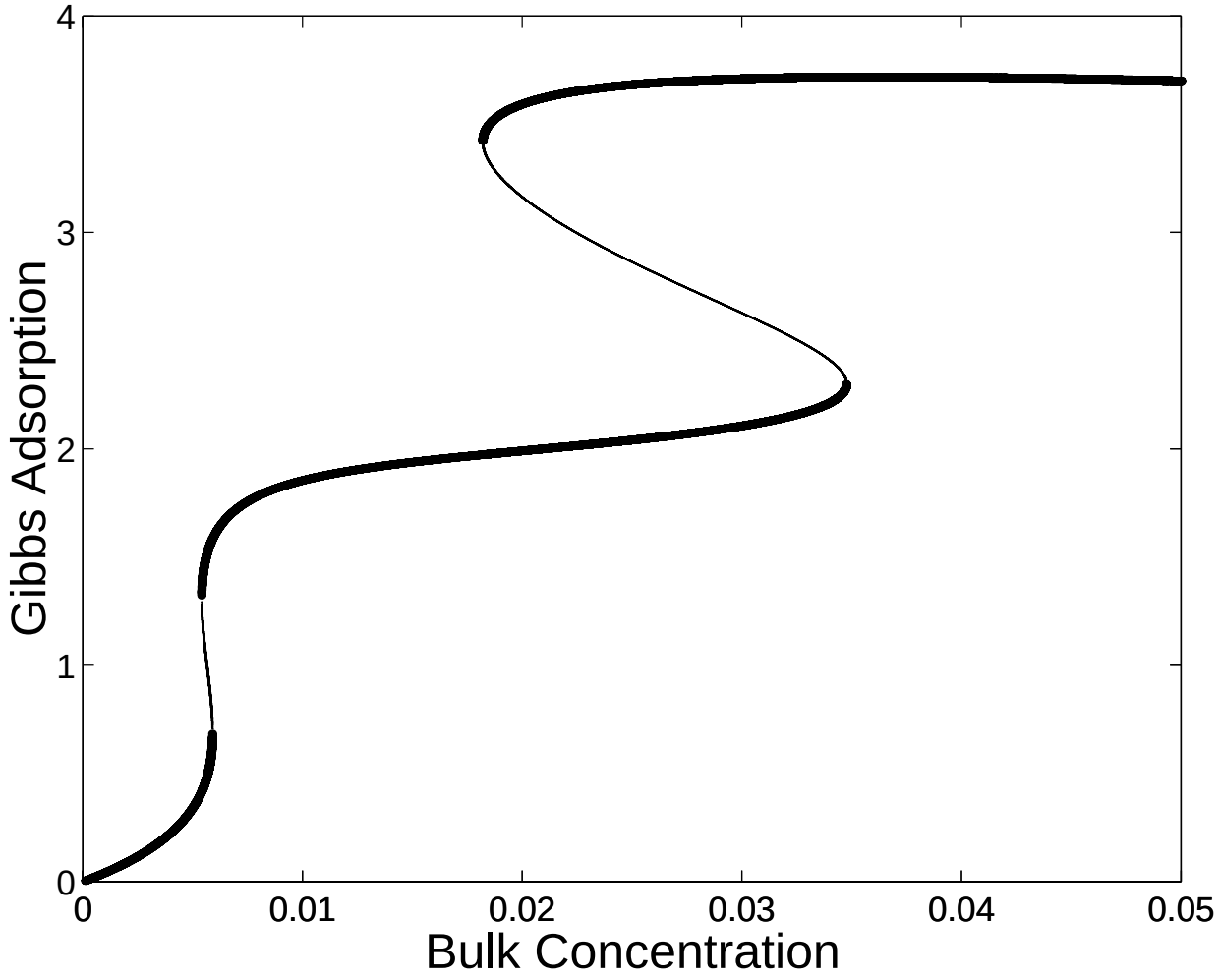

Figure 3: Results for four-layer problem with $z_1 = 1, z_2 = 4, E_{AA} = -1.1, E_{AS} = -3.0$. The bold lines indicate regions that are either stable or metastable. The thin lines indicate unstable regions.

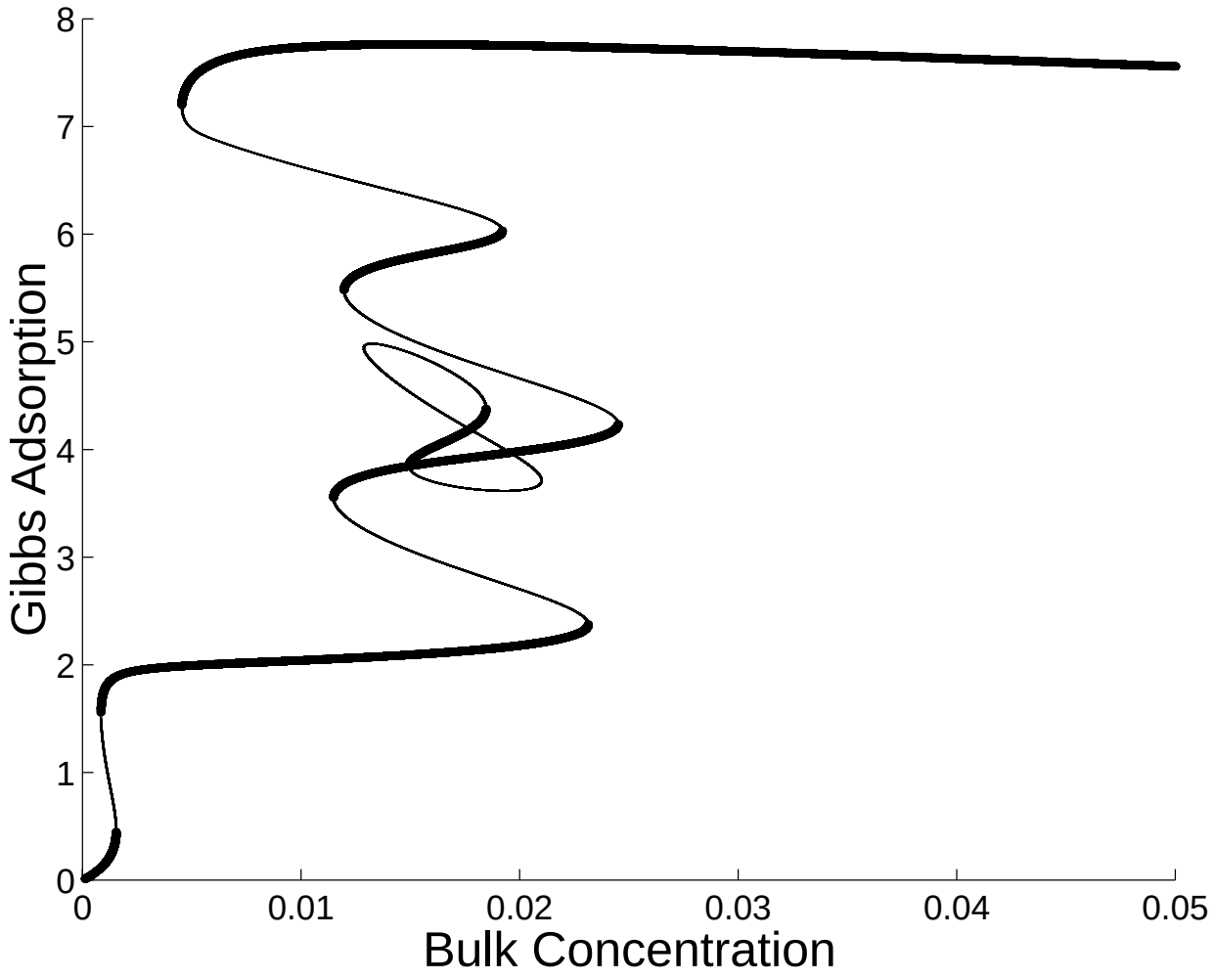

Figure 4: Results for eight-layer problem with $z_1 = 1, z_2 = 4, E_{AA} = -1.4, E_{AS} = -4.0$. The bold lines indicate regions that are either stable or metastable. The thin lines indicate unstable regions.

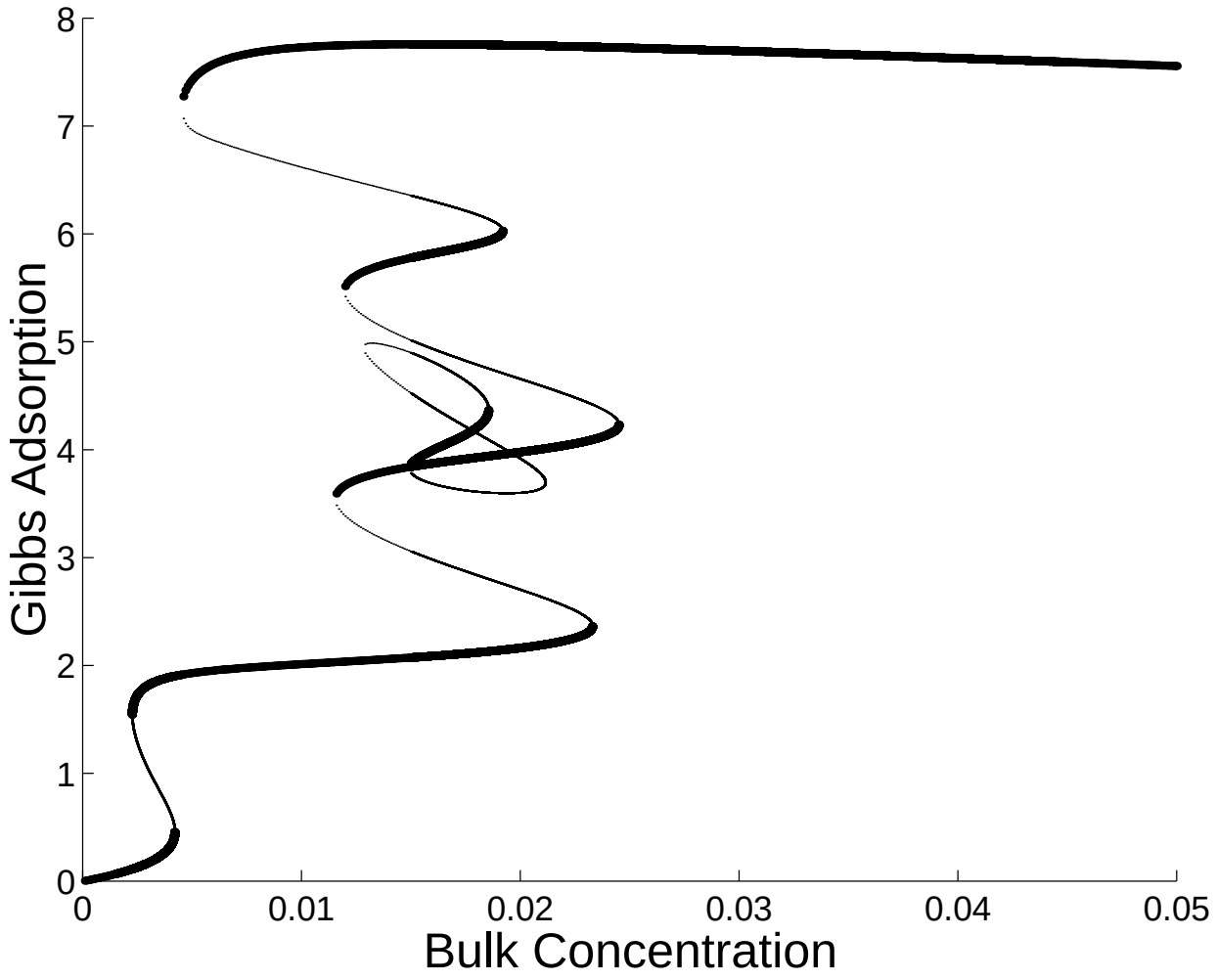

Figure 5: Results for eight-layer problem with $z_1 = 1, z_2 = 4, E_{AA} = -1.4, E_{AS} = -3.0$. The bold lines indicate regions that are either stable or metastable. The thin lines indicate unstable regions.

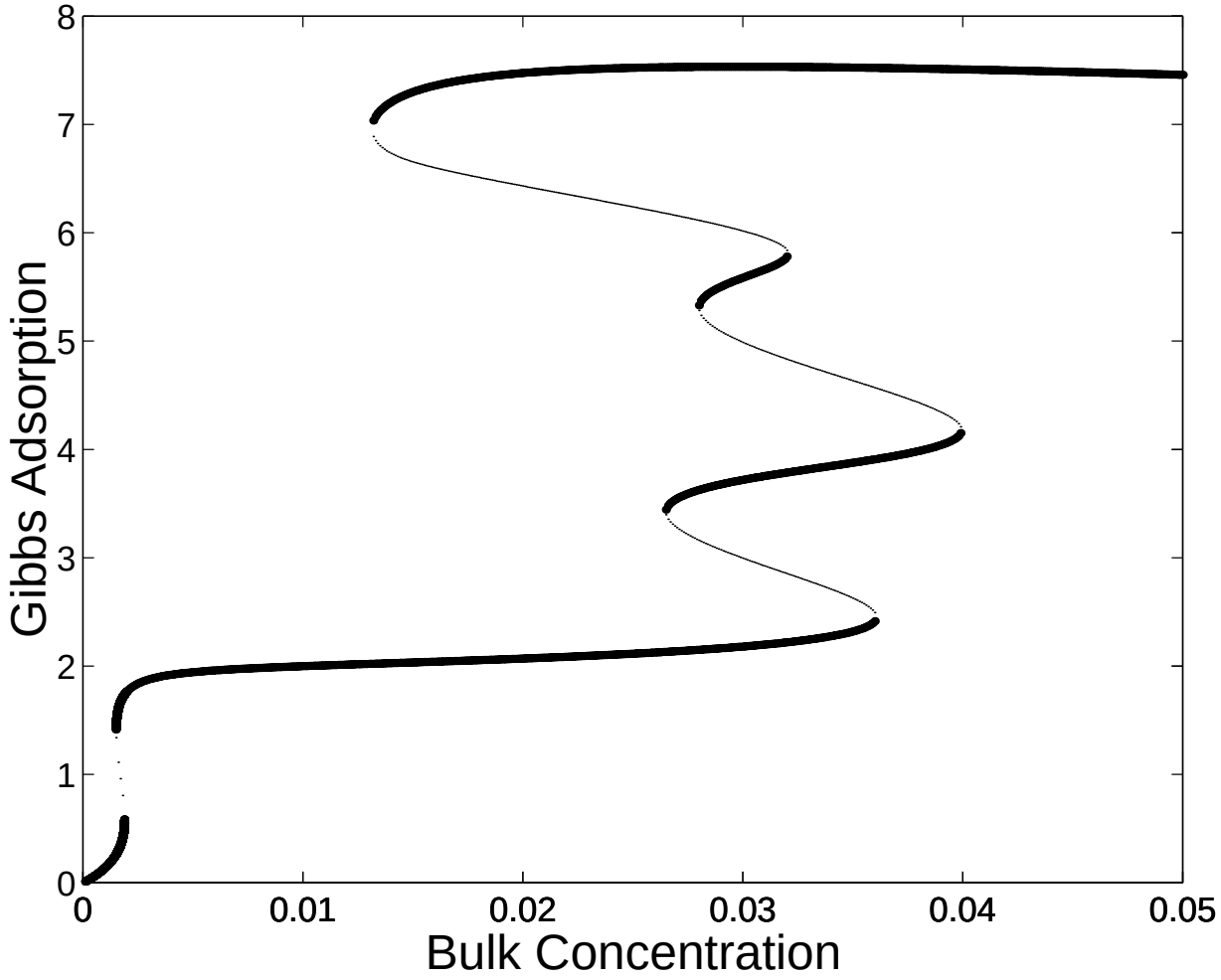

Figure 6: Results for eight-layer problem with $z_1 = 1, z_2 = 4, E_{AA} = -1.2, E_{AS} = -4.0$. The bold lines indicate regions that are either stable or metastable. The thin lines indicate unstable regions.

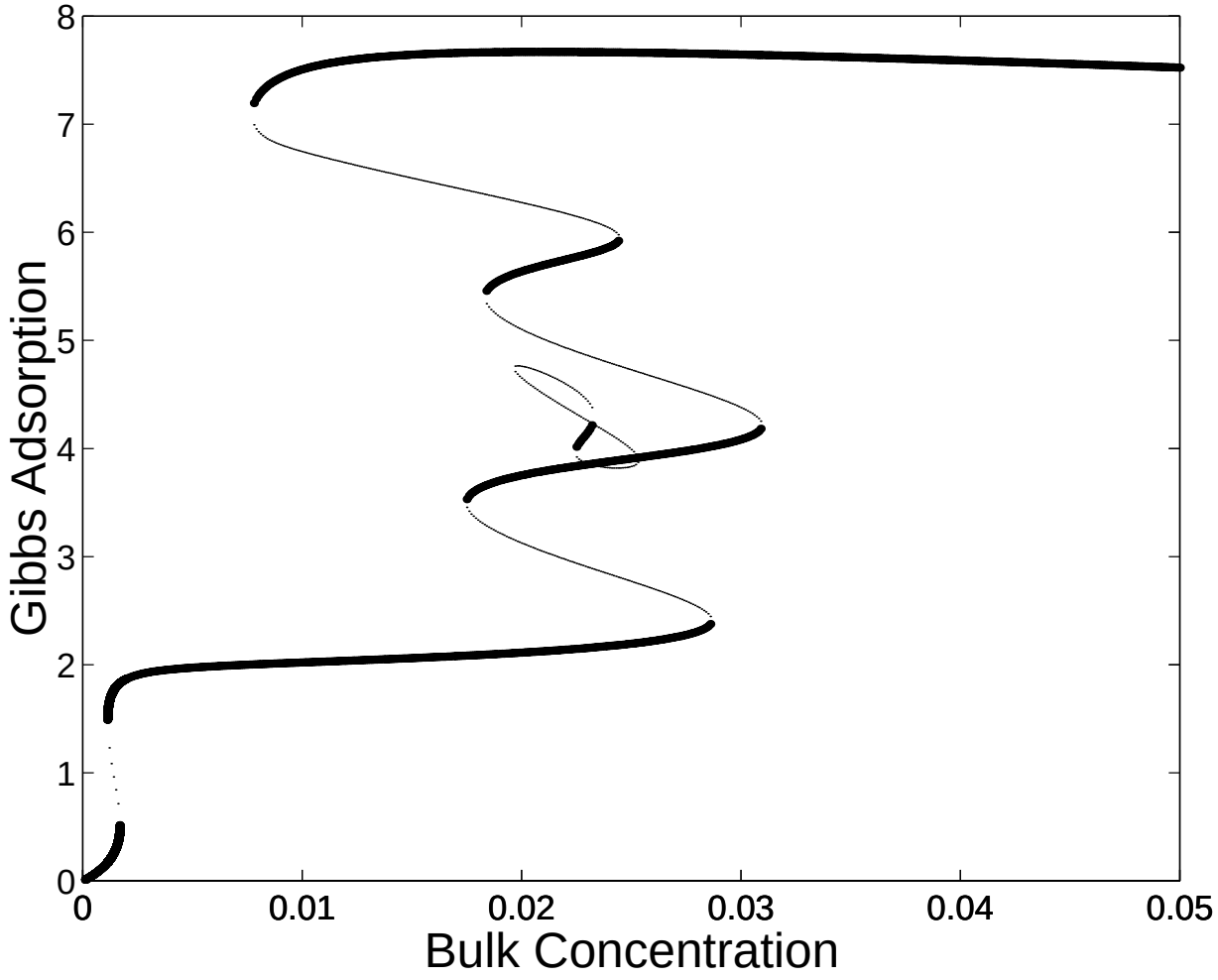

Figure 7: Results for eight-layer problem with $z_1 = 1, z_2 = 4, E_{AA} = -1.3, E_{AS} = -4.0$. The bold lines indicate regions that are either stable or metastable. The thin lines indicate unstable regions.

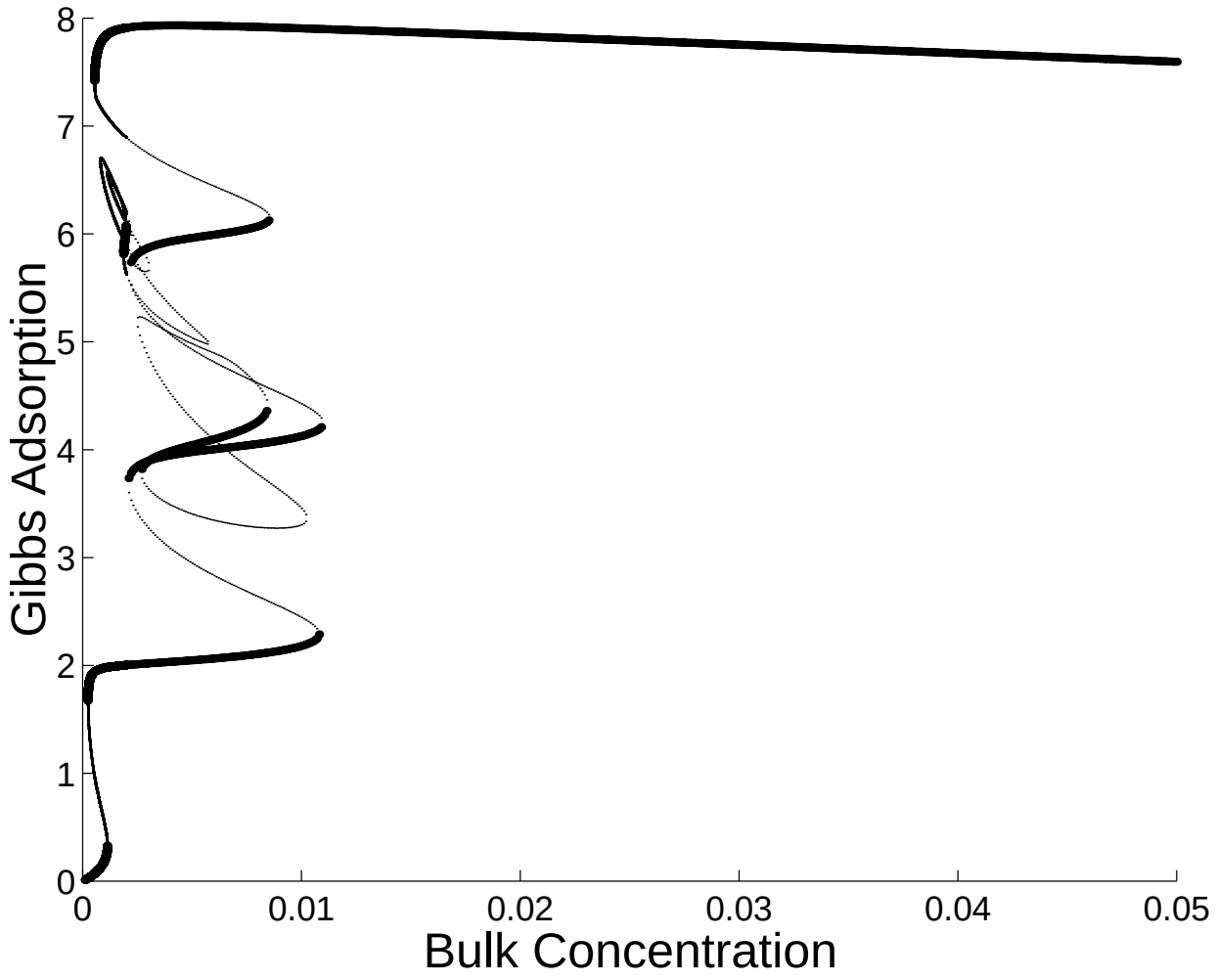

Figure 8: Results for eight-layer problem with $z_1 = 1, z_2 = 4, E_{AA} = -1.8, E_{AS} = -4.0$. The bold lines indicate regions that are either stable or metastable. The thin lines indicate unstable regions.

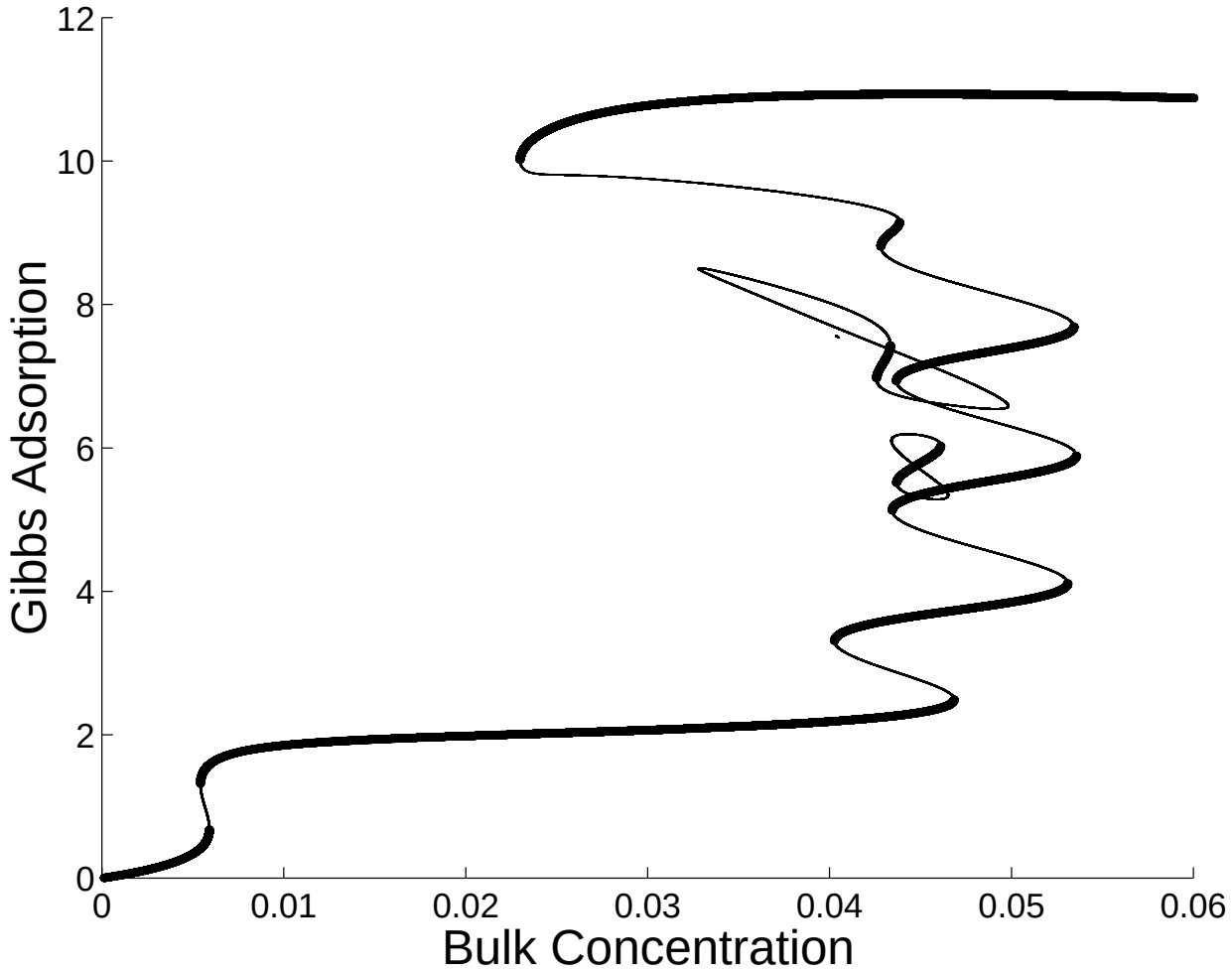

Figure 9: Results for 12-layer problem with $z_1 = 1, z_2 = 4, E_{AA} = -1.1, E_{AS} = -3.0$. The bold lines indicate regions that are either stable or metastable. The thin lines indicate unstable regions.

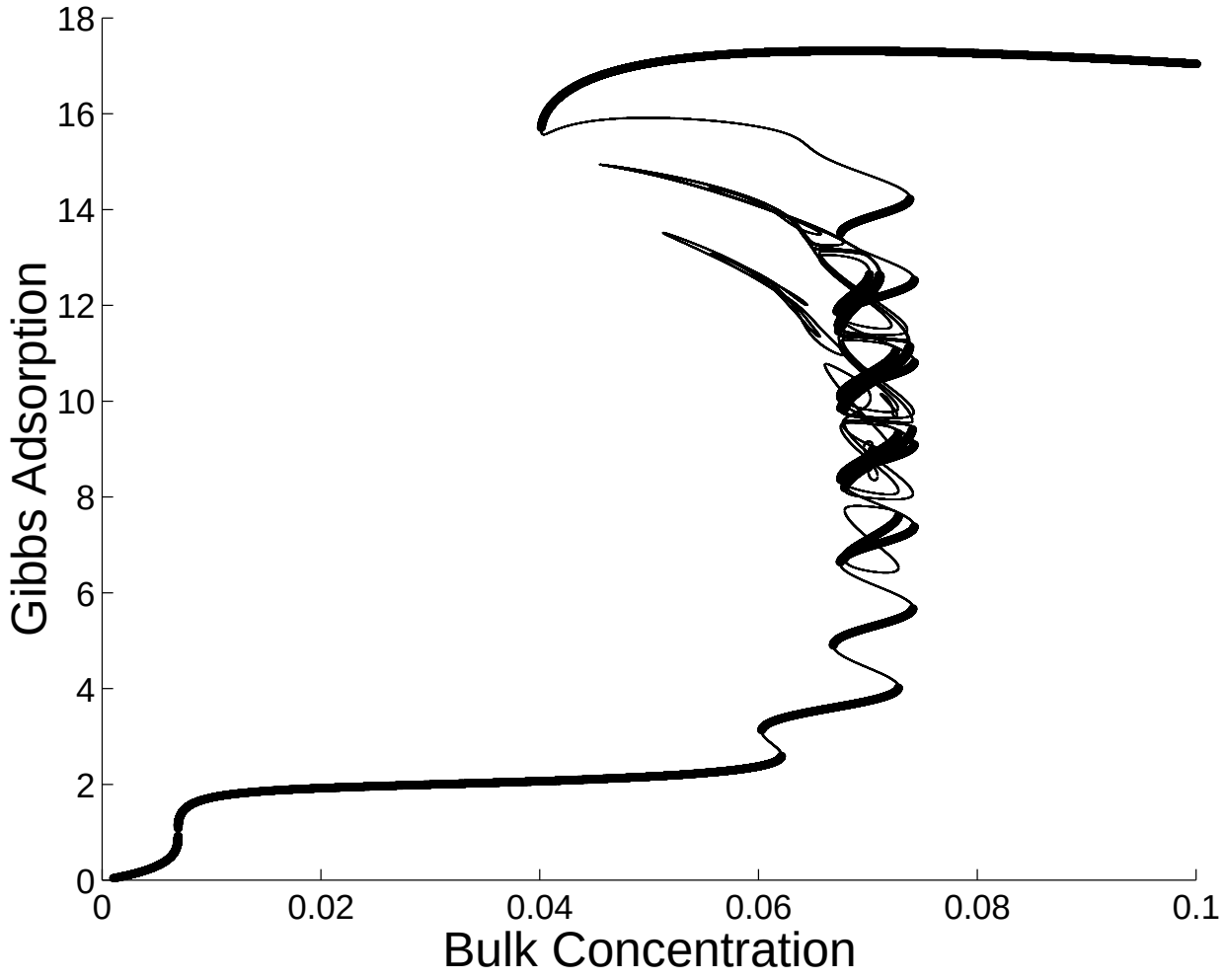

Figure 10: Results for 20-layer problem with $z_1 = 1, z_2 = 4, E_{AA} = -1.0, E_{AS} = -3.0$. The bold lines indicate regions that are either stable or metastable. The thin lines indicate unstable regions.

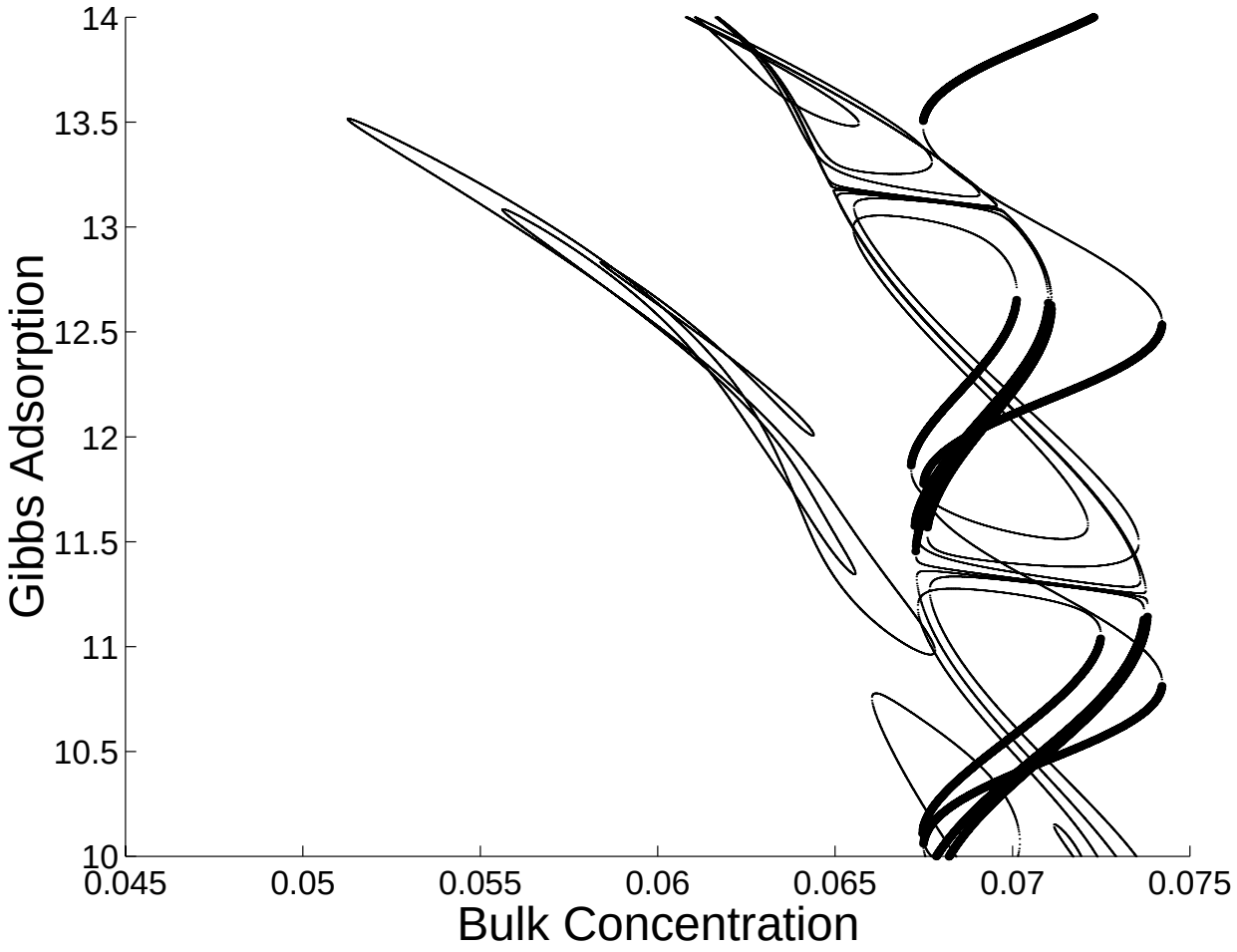

Figure 11: An expanded version of part of Figure 11 showing results for 20-layer problem. The bold lines indicate regions that are either stable or metastable. The thin lines indicate unstable regions.

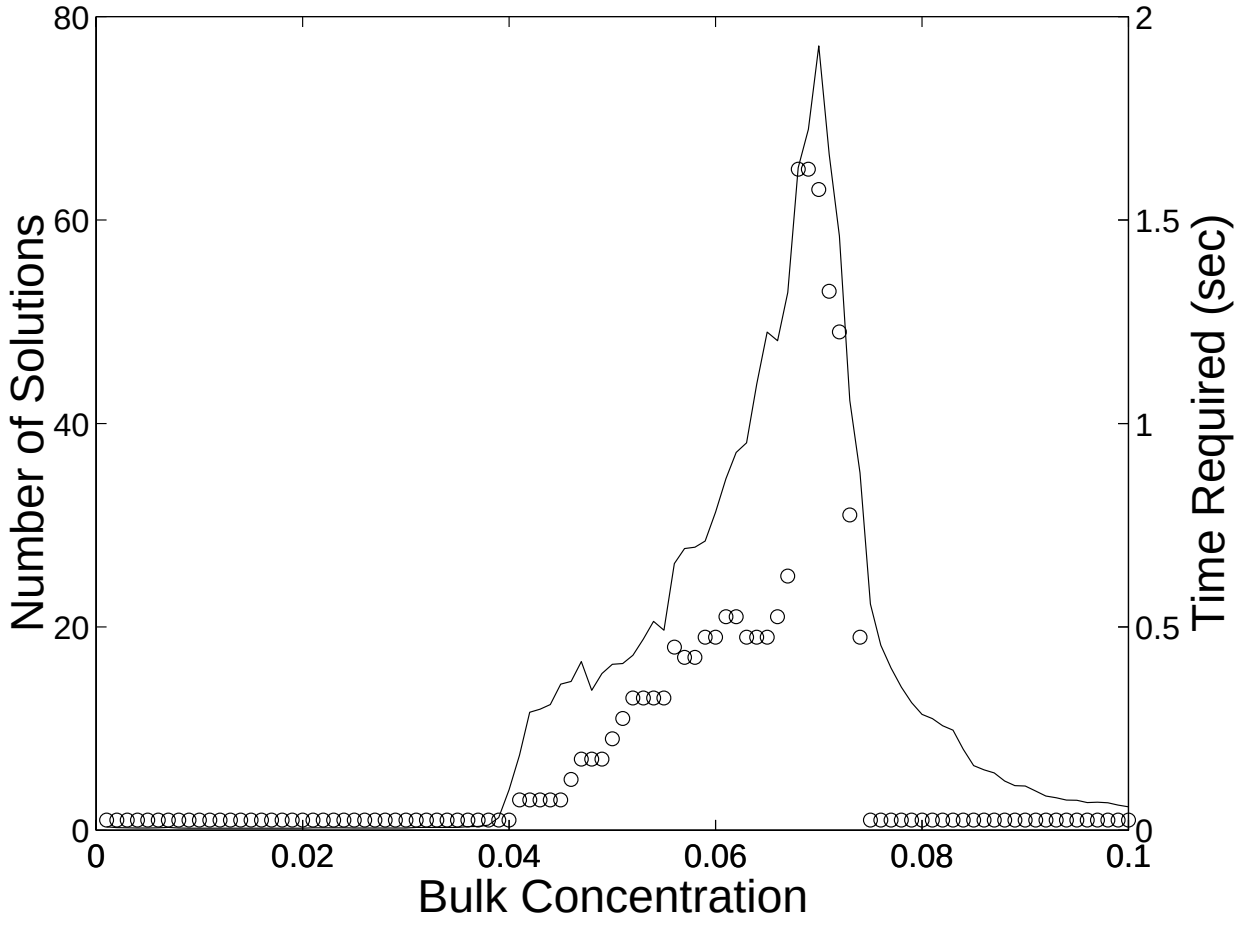

Figure 12: Number of roots and computational performance on the 20-layer problem. Circles correspond to the left axis, and indicates the number of solutions at a particular bulk concentration. The line corresponds to the right axis, and indicates the time required to completely solve the problem for all the roots.